

RESEARCH ARTICLE

Breadth and function of antibody response to acute SARS-CoV-2 infection in humans

Kuan-Ying A. Huang^{1,2*}, Tiong Kit Tan³, Ting-Hua Chen⁴, Chung-Guei Huang^{1,5}, Ruth Harvey⁶, Saira Hussain⁶, Cheng-Pin Chen⁷, Adam Harding⁸, Javier Gilbert-Jaramillo⁸, Xu Liu⁸, Michael Knight⁸, Lisa Schimanski^{3,9}, Shin-Ru Shih^{1,5}, Yi-Chun Lin¹⁰, Chien-Yu Cheng⁷, Shu-Hsing Cheng¹⁰, Yhu-Chering Huang², Tzou-Yien Lin², Jia-Tsong Jan⁴, Che Ma⁴, William James⁸, Rodney S. Daniels⁶, John W. McCauley⁶, Pramila Rijal^{3,9}, Alain R. Townsend^{3,9*}

1 Research Center for Emerging Viral Infections, College of Medicine, Chang Gung University, Taoyuan, Taiwan, **2** Division of Pediatric Infectious Diseases, Department of Pediatrics, Chang Gung Memorial Hospital, Taoyuan, Taiwan, **3** MRC Human Immunology Unit, Weatherall Institute of Molecular Medicine, University of Oxford, John Radcliffe Hospital, Oxford, United Kingdom, **4** Genomics Research Center, Academia Sinica, Taipei, Taiwan, **5** Department of Laboratory Medicine, Chang Gung Memorial Hospital, Taoyuan, Taiwan, **6** Worldwide Influenza Centre, The Francis Crick Institute, 1 Midland Road, London, United Kingdom, **7** Department of Infectious Diseases, Taoyuan General Hospital, Ministry of Health and Welfare, Taoyuan, and National Yang-Ming University, Taipei, Taiwan, **8** Sir William Dunn School of Pathology, University of Oxford, Oxford, United Kingdom, **9** Centre for Translational Immunology, Chinese Academy of Medical Sciences Oxford Institute, University of Oxford, Oxford, United Kingdom, **10** Department of Infectious Diseases, Taoyuan General Hospital, Ministry of Health and Welfare, Taoyuan, and Taipei Medical University, Taipei, Taiwan

☯ These authors contributed equally to this work.

* arthur1726@cgmh.org.tw (K-YAH); alain.townsend@imm.ox.ac.uk (ART)



OPEN ACCESS

Citation: Huang K-YA, Tan TK, Chen T-H, Huang C-G, Harvey R, Hussain S, et al. (2021) Breadth and function of antibody response to acute SARS-CoV-2 infection in humans. *PLoS Pathog* 17(2): e1009352. <https://doi.org/10.1371/journal.ppat.1009352>

Editor: Benhur Lee, Icahn School of Medicine at Mount Sinai, UNITED STATES

Received: November 22, 2020

Accepted: February 2, 2021

Published: February 26, 2021

Copyright: © 2021 Huang et al. This is an open access article distributed under the terms of the [Creative Commons Attribution License](https://creativecommons.org/licenses/by/4.0/), which permits unrestricted use, distribution, and reproduction in any medium, provided the original author and source are credited.

Data Availability Statement: The sequences of antibodies are available from the NCBI, with GenBank Accession numbers: MT943491-MT943518. All other relevant data are within the manuscript and its [Supporting Information](#) files.

Funding: This work was mainly supported by the grant from Chang Gung Memorial Hospital (BMRPE22) to KYAH. This work was partially supported by the Fast Grant (BRD00230-CF01) to ART, the Chinese Academy of Medical Sciences (GAMS) Innovation Fund for Medical Science

Abstract

Serological and plasmablast responses and plasmablast-derived IgG monoclonal antibodies (MAbs) have been analysed in three COVID-19 patients with different clinical severities. Potent humoral responses were detected within 3 weeks of onset of illness in all patients and the serological titre was elicited soon after or concomitantly with peripheral plasmablast response. An average of 13.7% and 3.5% of plasmablast-derived MAbs were reactive with virus spike glycoprotein or nucleocapsid, respectively. A subset of anti-spike (10 of 32) antibodies cross-reacted with other betacoronaviruses tested and harboured extensive somatic mutations, indicative of an expansion of memory B cells upon SARS-CoV-2 infection. Fourteen of 32 anti-spike MAbs, including five anti-receptor-binding domain (RBD), three anti-non-RBD S1 and six anti-S2, neutralised wild-type SARS-CoV-2 in independent assays. Anti-RBD MAbs were further grouped into four cross-inhibiting clusters, of which six antibodies from three separate clusters blocked the binding of RBD to ACE2 and five were neutralising. All ACE2-blocking anti-RBD antibodies were isolated from two recovered patients with prolonged fever, which is compatible with substantial ACE2-blocking response in their sera. Finally, the identification of non-competing pairs of neutralising antibodies would offer potential templates for the development of prophylactic and therapeutic agents against SARS-CoV-2.

(CIFMS), China (2018-I2M-2-002) to TKT, PR, LS and ART, the EPA Cephalosporin Fund and The Townsend–Jeantet Charitable Trust (charity no. 1011770) to TKT, Cancer Research UK (FC001030), the Medical Research Council (FC001030) and the Wellcome Trust (FC001030) to JWM, and the University of Oxford's COVID-19 Research Response Fund to ART. The funders had no role in study design, data collection and analysis, decision to publish, or preparation of the manuscript.

Competing interests: I have read the journal's policy and the authors of this manuscript have the following competing interests: KYAH files a patent application on anti-spike and anti-nucleocapsid antibodies described herein.

Author summary

The global COVID-19 outbreak poses a serious threat to human health and antibody-mediated immunity plays a key role in controlling acute viral infection in humans. We report the complete mapping of antibody responses, from serology through to single plasmablast-derived antibody clone, in three COVID-19 patients with different severities. The data show that a subset of anti-spike plasmablast-derived antibodies cross-react with other betacoronaviruses including human coronavirus OC43, which suggests an expansion of memory B cells upon SARS-CoV-2 infection. Anti-SARS-CoV-2 spike antibody clones target a diverse spectrum of epitopes on the receptor-binding domain (RBD), non-RBD S1 and S2 regions of the spike glycoprotein, 40% of them neutralise wild-type SARS-CoV-2. Anti-RBD antibodies constitute a major part of neutralising antibody response. Potent antibodies target three non-overlapping epitopes on the RBD, and the neutralising activity is linked to ACE2-binding blockade. Combinations of multiple antibody clones targeting non-overlapping epitopes offer a potential avenue to combat the global outbreak.

Introduction

In late 2019, a novel coronavirus emerged and was identified as the cause of a cluster of respiratory infection cases in Wuhan, China. It spread quickly around the world. In March of 2020 a pandemic was declared by the World Health Organization, the virus was formally named as Severe Acute Respiratory Syndrome Coronavirus 2 (SARS-CoV-2) and the resulting disease was named COVID-19. As of 1 April 2021, there have been over 128 million confirmed cases of SARS-CoV-2 infection with over two million deaths (World Health Organization, <https://covid19.who.int/>).

There is no fully effective drug for COVID-19. Antibodies neutralise SARS-CoV-2 *in vitro*, consistent with the induction of neutralising antibodies and protection from disease seen after vaccination [1,2], and antibodies may be an effective treatment for COVID-19 in clinical practice. Convalescent plasma is being tested in clinical trials as a therapy for COVID-19 [3,4], and may be effective if given early after infection [5]. It was previously used in the treatment of SARS [6]. The virus spike, a trimeric glycoprotein on the viral surface, is a target of neutralising antibodies, and plays a central role in receptor binding and membrane fusion. The spike is composed of two functional subunits; the S1 subunit contains the receptor-binding domain (RBD) that is required for binding to host cell ACE2 receptor and the N-terminal domain (NTD) and the S2 subunit mediates the fusion of the viral and host cell membranes [7].

B cell responses in COVID-19 patients have been detected concomitantly with follicular helper T cell responses from week one after illness onset [8]. In SARS patients, B cell responses typically arise first against the nucleocapsid protein then, within four to eight days after symptom onset, antibody responses to spike glycoprotein have been found; neutralising antibody responses begin to develop by week two, and most symptomatic patients develop neutralising antibodies by week three [9]. Two serological studies of COVID-19 patients showed anti-SARS-CoV-2 IgG seroconversion at week three after onset and some cross-reactivity to nucleocapsid of SARS [10,11].

Antibodies may play a role in protection against SARS-CoV-2 infection. The underlying B-cell response leading to the rapid production of plasmablasts (antibody-secreting cells) that secrete antibodies upon natural SARS-CoV-2 exposure/infection is only beginning to be

understood [8]. Here, we characterised the infection-induced serological and plasmablast responses and the derived IgG anti-SARS-CoV-2 spike glycoprotein and nucleocapsid monoclonal antibodies (MAbs) from adult patients with laboratory-confirmed COVID-19. The antigenic specificity and breadth of antibodies and the sequence of their variable domains have been characterised in detail. Virus neutralising antibodies were detected that bound epitopes on receptor-binding domain, non-RBD regions of the S1 polypeptide, and the S2 polypeptide of the spike glycoprotein.

Results

Serological response and anti-spike glycoprotein and anti-nucleocapsid IgG antibodies from circulating plasmablasts

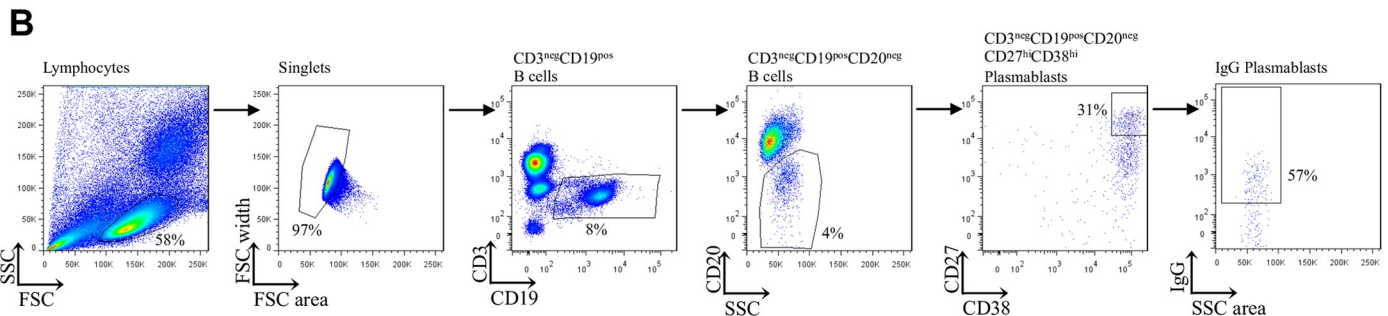
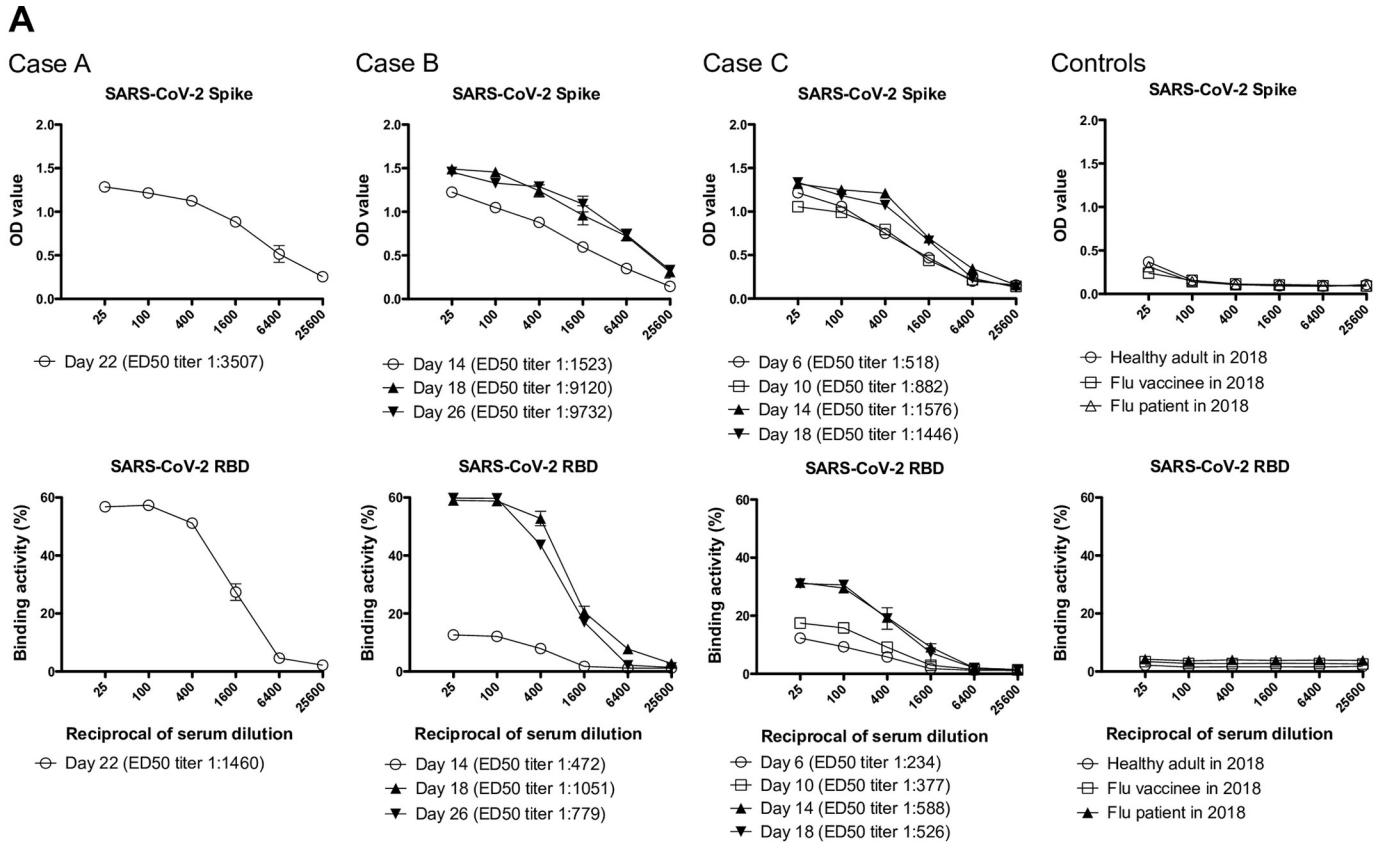
Serum IgG antibodies to the virus spike glycoprotein and the isolated RBD were analysed by indirect enzyme-linked immunosorbent and flow cytometry assays in three patients with laboratory-confirmed COVID-19. The clinical characteristics of the three patients studied are shown in [S1 Table](#). Antibodies to spike glycoprotein and RBD were detected in all three patients after week 3 of illness onset ([Fig 1A](#)). Case A showed a robust response to spike glycoprotein and the isolated RBD by day (D) 22 (D22). Longitudinal sera from case B and C showed lower anti-spike glycoprotein and RBD IgG titres at week 1 or the beginning of week 2 and an elevated titre that peaked at the end of week 2 through week 3 (a peak 50% effective dilution (ED_{50}) titre to RBD 1:1,051 at D18 in case B and 1:588 at D14 in case C). Case B had prolonged fever and developed pneumonia at the end of week 2, which was followed by a robust increase of anti-spike glycoprotein and RBD IgG titres at week 3 ([Fig 1A](#), [S1 Table](#)). By contrast, case C experienced a two-day course of febrile illness and reduction of all symptoms within the first week, followed by anti-spike glycoprotein and RBD IgG titres that peaked earlier at the end of week 2 ([Fig 1A](#), [S1 Table](#)).

An increased frequency of circulating plasmablasts was detected in all three patients (healthy adults baseline less than 1%) [8] ([Fig 1B](#)). In case A, a plasmablast response containing a substantial IgG subset was detected at the end of week 2 (D14), followed by a high serological titre at week 3 (D22). Case B had a robust plasmablast response at the end of week 2 (D14) but the IgG plasmablast subset continued to rise, dominated at week 3 (D18), but then subsided at the beginning of week 4 (D22), which is compatible with high anti-spike glycoprotein and RBD IgG serological titres at week 3. Case C produced a significant early plasmablast response at the end of week 1 (D6), the IgG plasmablast subset dominated at the same time, and both the plasmablast response and its IgG subsets subsided at the end of week 2 (D14).

Circulating plasmablasts were identified and used to generate human IgG monoclonal antibodies (MAbs) from the three patients ([Fig 2A](#)). A total of 219 plasmablast-derived IgG MAbs were produced, of which 40 (5 of 50 from case A, 27 of 131 from case B, 8 of 38 from case C) were shown to bind spike glycoprotein or nucleocapsid antigens of SARS-CoV-2 by one or more of the following: staining of spike glycoprotein, RBD and NTD-expressing cells, ELISA, or immunofluorescence and specific virus neutralisation ([Table 1](#)). Averages of $13.7 \pm 6.8\%$ (6.0–18.4%) and $3.5 \pm 0.8\%$ (2.6–4.0%) of plasmablast-derived IgG MAbs were reactive with virus spike glycoprotein and nucleocapsid, respectively.

Genetic and phenotypic characteristics of anti-spike glycoprotein antibodies

Among 32 anti-spike MAbs, 10 bound to the RBD, 13 to non-RBD S1, and the other 9 to the S2 subunit of the SARS-CoV-2 spike glycoprotein ([Table 1](#), [Fig 2A](#)). Twenty-four of these



Case	Onset date	Plasmablasts of CD3 ^{neg} CD19 ^{pos} B cells (%)	
		of B cells (%)	of Plasmablasts (%)
A	D14	1.99	0.34
	D18	37.48	1.67
	D22	1.13	0.64
B	D14	0.20	0.05
	D18	1.13	0.64
	D22	0.20	0.05
C	D2	2.56	0.11
	D6	2.09	0.97
	D14	0.83	0.09

Fig 1. The IgG serology and plasmablast response to acute SARS-CoV-2 infection among enrolled patients. (A) The binding activity of post-infection sera IgG with SARS-CoV-2 spike glycoprotein in an ELISA and SARS-CoV-2 RBD assessed by flow cytometry on transduced cells, among enrolled patients. Each experiment was repeated twice. Values are presented as mean \pm standard error of the mean. Two sera from healthy adults (one collected at day 28 post 2018–19 influenza vaccination and one collected from an influenza-infected patient 9 days after symptom onset) in 2018 were included as controls. Linear regression was used to determine the 50% end-point dilution (ED₅₀). (B) The gating strategy used for peripheral total B cells, plasmablasts and IgG plasmablasts in flow cytometry. The frequency of circulating plasmablasts (percentage of total B cells) among enrolled cases was measured by flow cytometry. Onset date (D = Day).

<https://doi.org/10.1371/journal.ppat.1009352.g001>

MAbs bound to virus antigens as assessed by immunofluorescence of SARS-CoV-2-infected Vero E6 cells (S1 Fig, Table 1), suggesting that the majority of anti-spike glycoprotein human antibodies recognise complex conformational epitopes on the virus glycoprotein.

Moderate binding was observed for a subset (4 of 9) of anti-S2 MAbs with full-length spike glycoprotein ectodomain in the indirect ELISA but bound strongly to the isolated S2 subunit (Fig 2B). All anti-S2 MAbs bound to the MDCK-SIAT1 cells transduced to express the prefusion-stabilized spike antigen (S2 Fig).

Ten of 32 anti-SARS-CoV-2 spike glycoprotein MAbs cross-reacted with the glycoproteins of other betacoronaviruses, including SARS, Middle East Respiratory Syndrome coronavirus (MERS) or human common cold coronavirus OC43 in ELISA (Table 1), suggesting the presence of conserved epitopes on the spike glycoproteins of betacoronaviruses [12–14].

Each of 32 anti-spike glycoprotein MAbs was encoded by a unique set of heavy chain VDJ and light chain VJ rearrangements in the variable domain (S2 Table). Fourteen of 32 SARS-CoV-2 spike-reactive MAb genes possessed low numbers of somatic mutations resulting in 0 or 1 amino acid substitutions suggesting a *de novo* B cell response to the SARS-CoV-2 virus in humans. Six of the 32 MAb genes possessed ≥ 20 nucleotide mutations, and these cross-reacted on other beta-coronaviruses, including OC43. Of the nine anti-S2 antibodies five cross-reacted on OC43 virus and three of these also cross-reacted on MERS (Table 1). All five cross-reactive anti-S2 antibodies had high rates of somatic mutation (25 ± 5), indicating a memory phenotype.

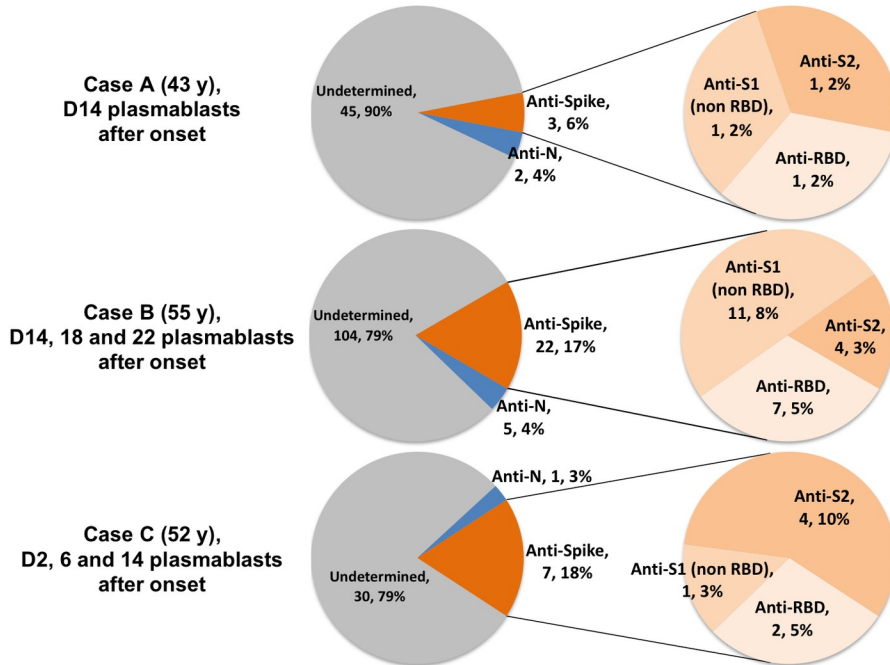
The CDR3 length varied among anti-spike glycoprotein antibodies (S2 Table). No significant differences were found between anti-S2 and anti-S1 or anti-RBD subsets. Among anti-S2 MAbs, a significantly longer heavy chain CDR3 length was found in the cross-reactive group compared to the specific group (Cross-reactive 20 ± 2 versus Specific 12 ± 4 , $p = 0.02$, two-tailed Mann-Whitney test; Fig 2C), indicating that a long CDR3 may play a role in antigen binding, which is also found in several broadly reactive human MAbs against human immunodeficiency virus and influenza virus [15,16].

The relationship of the binding activity to CDR3 length of anti-RBD MAbs was further characterised in detail. Using MDCK-SIAT1 cells transduced to express the RBD at the cell surface (by linkage to a transmembrane domain from Influenza haemagglutinin) and flow cytometry, binding activities of the anti-RBD MAbs were shown to vary with 50% binding concentration from 0.10 to 1.70 $\mu\text{g/ml}$ (S3 Fig). The MAbs with strong anti-RBD binding have a relatively long heavy chain CDR3 length (50% binding concentration $< 0.5 \mu\text{g/ml}$ versus $> 0.5 \mu\text{g/ml}$, $p = 0.03$, two-tailed Mann-Whitney test; S4 Fig).

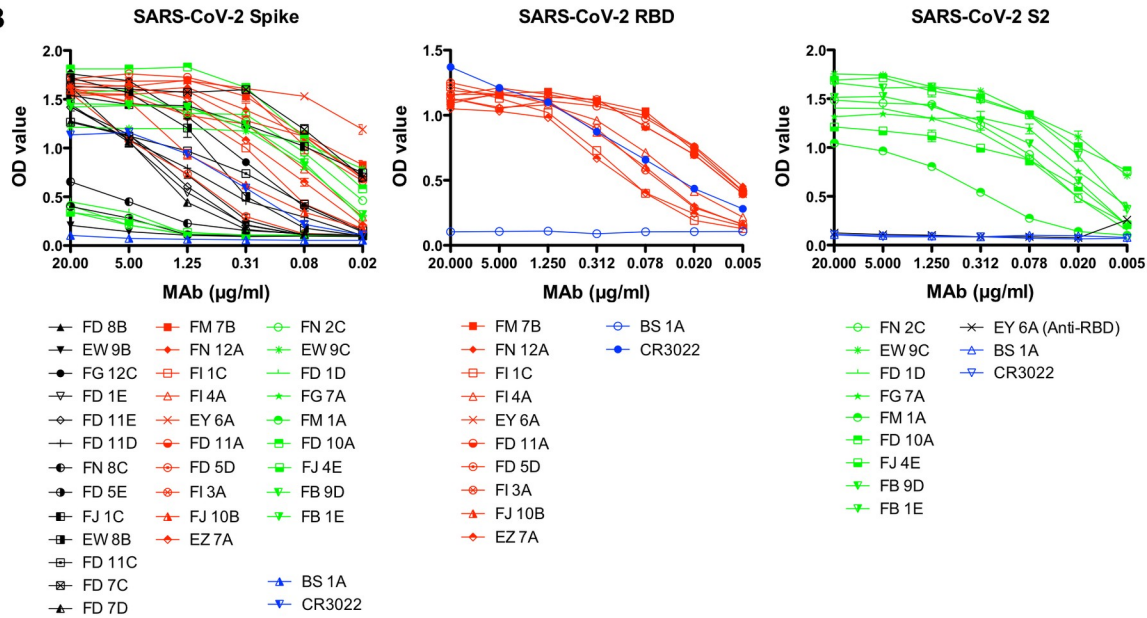
Neutralisation by anti-spike glycoprotein antibodies

The 32 anti-spike glycoprotein MAbs were systematically examined by plaque reduction neutralisation (PRNT) assay for neutralisation of wild-type SARS-CoV-2 virus (see methods, Table 1). A total of 14 neutralising antibodies distributed between different regions of the spike glycoprotein were identified: 5 of 10 to RBD, 3 of 13 to S1 (non-RBD), 6 of 9 to S2. The EC₅₀ concentrations, as a measure of potency, ranged from 0.05 to $\sim 133 \text{ nM}$ (8 ng/ml— $\sim 20 \mu\text{g/ml}$).

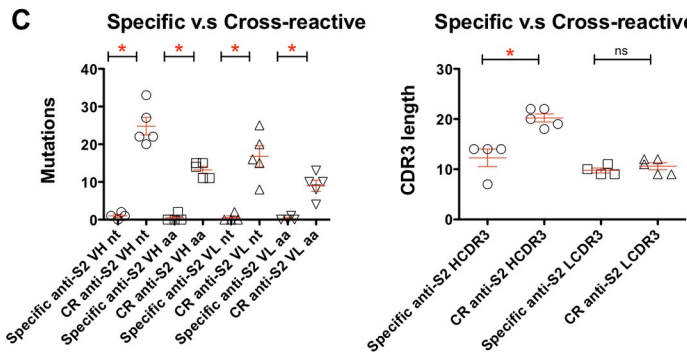
A



B



C



D

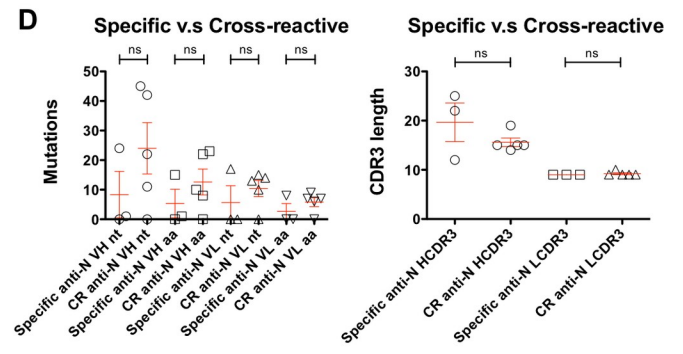


Fig 2. Plasmablast-derived IgG monoclonal antibodies from three COVID-19 patients. (A) A total of 219 IgG monoclonal antibodies were produced from COVID-19 patients (50 from case A, 131 from case B, 38 from case C). An average of $13.7 \pm 6.8\%$ and $3.5 \pm 0.8\%$ of antibodies were reactive with spike glycoprotein (S) and nucleocapsid (N) antigens of SARS-CoV-2, respectively. The data are presented as specificity, number of antibodies, and the percentage of total antibodies isolated from each patient. (B) The binding activity of anti-SARS-CoV-2 MAbs with spike glycoprotein, RBD and the S2 subunit in ELISA. Anti-influenza H3 MAb BS-1A and anti-SARS RBD CR3022 were included as controls. Each experiment was repeated twice. The OD_{450} values are presented as mean \pm standard error of the mean. Panels (C) and (D) show numbers of variable domain mutations in MAb genes and variation in MAb CDR3 lengths among anti-S2 and anti-N MAbs, respectively. Antibodies that strongly cross-react with at least one betacoronavirus (SARS or MERS or OC43) were defined as cross-reactive MAbs. CDR3 length and mutation numbers are presented as mean \pm standard error of the mean (anti-S2, specific, $n = 4$ versus cross-reactive, $n = 5$; anti-N, specific, $n = 3$ versus cross-reactive, $n = 5$). The two-tailed Mann-Whitney test was performed to compare the mutations between two groups. * $p < 0.05$; D, = Day; ns, non-significant; CR, cross-reactive.

<https://doi.org/10.1371/journal.ppat.1009352.g002>

Neutralisation of anti-RBD antibodies was corroborated by a microneutralisation test that measured a reduction in fluorescent focus-forming units (see [methods](#), [S5 Fig](#)). A selection of MAbs were also tested by a PCR-based neutralisation assay (see [methods](#)) and inhibition of virus replication was measured by quantitative PCR in the supernatant bathing the infected cells. This result corroborated that anti-RBD FD 11A, anti-RBD FI 3A, anti-RBD FD 5D, anti-RBD EY 6A and anti-S2 EW 9C, as crude culture supernatants, reduced the virus signal from ~ 56 - to $\sim 10,085$ -fold ([S6 Fig](#)).

ACE2 blockade by anti-RBD antibodies

Potent neutralising antibodies to the RBD of SARS-CoV-2 spike glycoprotein were identified and we then analysed the blockade of the ACE2-RBD interaction by anti-RBD antibodies in two assays ([Fig 3](#), [Table 1](#)), including an assay that we reported previously [[17](#),[18](#)]. In the first assay unlabelled MAbs in at least 10-fold excess were mixed with biotin labelled ACE2-Fc and binding to the RBD, displayed on RBD-VLP [[19](#)] bound to an ELISA plate ([Fig 3A](#), [S7 Fig](#)). The RBD-VLP was used to display the RBD on the plate, because direct binding of RBD to the ELISA plate resulted in loss of ACE2 binding ([S7 Fig](#)). Anti-RBD neutralising antibodies FI 3A and FI 1C, as well as the unlabelled ACE2-Fc, strongly inhibited the binding of labelled ACE2-Fc to RBD. A partial inhibition was detected by anti-RBD antibodies FD 11A, FD 5D and FI 4A. Another unlabelled nanobody VHH72-Fc in excess inhibited the binding of labelled ACE2-Fc to RBD in this assay. VHH72-Fc binds in the Class 4 region of the RBD [[20](#)], and competes for binding with the characterised MAbs CR3022 and EY 6A ([Table 1](#)) [[21–23](#)]. The structure of VHH72-Fc bound to RBD is known [[24](#)] and its footprint on the RBD does not overlap that of ACE2, so inhibition is thought to occur by steric hindrance.

In the second assay, we employed MDCK-SIAT1 cells overexpressing full-length human ACE2 as a transmembrane protein. Unlabelled antibodies or ACE2-Fc were mixed in excess with biotinylated RBD, and binding of RBD was detected with Streptavidin-HRP in ELISA ([Fig 3B](#)). The results of this assay mostly mirrored those of the first assay and confirmed that in this orientation anti-RBD neutralising antibodies FD 11A and FD 5D competed in excess with soluble RBD for binding to ACE2 ([Fig 3B](#)). In addition, anti-RBD neutralising antibody EY 6A competed with RBD for ACE2 binding. The binding pattern of EY 6A is analogous to a previously described antibody CR3022 ([Table 1](#)) [[21–23](#)]. These two antibodies are known to bind to the same region of RBD away from the ACE2 binding site, but they influence the binding kinetics of RBD to ACE2, presumably through steric effects [[18](#)].

Division of anti-RBD antibodies into cross-inhibiting groups

The ten anti-RBD MAbs were then divided into cross-inhibiting groups as described for human MAbs to Ebola [[25](#)] by assessing competition of unlabelled antibodies at 10-fold (or greater) excess over a biotin labelled target antibody by ELISA. Included as controls were the VHH72-Fc [[24](#)] and H11-H4-Fc [[17](#)] nanobodies linked to the hinge and Fc region of human

Table 1. The antigenic specificity, cross-reactivity and function of 32 anti-SARS-CoV-2 spike monoclonal antibodies derived from COVID-19 patients.

RBD-specific														
MAb	Case	FCM ^a			IFA ^b	SARS-CoV-2 ^c			Cross-reactivity ^c			PRNT ^d EC ₅₀ (nM)	ACE2-block ^e	
		S	RBD	NTD		S	RBD	S2	SARS	MERS	OC43		RBD anchored	ACE2 anchored
FD 11A	B	pos	pos	-ve	pos	1.64	1.17	0.13	0.1	0.1	0.12	0.05	+	++
FI 3A	B	pos	pos	-ve	pos	1.6	1.12	0.12	0.08	0.08	0.09	8.67	++++	++++
FI 1C	B	pos	pos	-ve	pos	1.88	1.22	0.16	0.15	0.15	0.18	16.67	++++	++
FD 5D	B	pos	pos	-ve	pos	1.83	1.19	0.13	0.09	0.1	0.09	133.33	+	+++
EY 6A	A	pos	pos	-ve	pos	1.75	1.18	0.13	1.82	0.12	0.11	133.33	-ve	++
FI 4A	B	pos	pos	-ve	pos	1.68	1.12	0.12	0.08	0.09	0.1	-ve	+	-ve
EZ 7A	B	pos	pos	-ve	pos	1.66	1.12	0.33	1.56	0.1	0.11	-ve	-ve	-ve
FJ 10B	B	pos	pos	-ve	-ve	1.48	1.22	0.13	1.26	0.1	0.14	-ve	-ve	-ve
FM 7B	C	pos	pos	-ve	pos	1.8	1.27	0.12	2.25	0.09	0.1	-ve	-ve	-ve
FN 12A	C	pos	pos	-ve	pos	2.24	1.33	0.3	0.36	0.29	0.38	-ve	-ve	-ve
S1-non-RBD														
MAb	Case	FCM ^a			IFA ^b	SARS-CoV-2 ^c			Cross-reactivity ^c			PRNT ^d EC ₅₀ (nM)		
		S	RBD	NTD		S	RBD	S2	SARS	MERS	OC43			
FJ 1C	B	pos	-ve	pos	pos	1.61	0.27	0.15	0.23	0.15	0.16	55.5		
FD 11E	B	pos	-ve	-ve	pos	1.45	0.11	0.12	0.11	0.12	0.14	70		
FD 1E	B	pos	-ve	-ve	pos	1.45	0.11	0.13	0.12	0.12	0.14	110		
EW 8B	B	pos	-ve	-ve	-ve	1.61	0.11	0.13	0.11	0.11	0.12	-ve		
FD 11D	B	pos	-ve	pos	pos	1.42	0.18	0.22	0.42	0.25	0.29	-ve		
FD 11C	B	pos	-ve	-ve	pos	1.2	0.14	0.2	0.11	0.11	0.12	-ve		
FD 7D	B	pos	-ve	-ve	-ve	1.44	0.12	0.14	0.11	0.11	0.12	-ve		
FD 8B	B	pos	-ve	-ve	-ve	1.1	0.14	0.12	0.08	0.1	0.09	-ve		
FD 7C	B	pos	-ve	pos	pos	1.9	0.15	0.15	0.13	0.12	0.13	-ve		
FG 12C	A	pos	-ve	-ve	pos	1.74	0.14	0.11	0.08	0.08	0.1	-ve		
FN 8C	C	pos	-ve	-ve	-ve	0.54	0.16	0.16	0.11	0.09	0.12	-ve		
FD 5E	B	pos	-ve	-ve	pos	0.34	0.16	0.16	0.13	0.11	0.11	-ve		
EW 9B	B	pos	-ve	-ve	-ve	0.22	0.17	0.11	0.09	0.1	0.09	-ve		
S2-specific														
MAb	Case	FCM ^a			IFA ^b	SARS-CoV-2 ^c			Cross-reactivity ^c			PRNT ^d EC ₅₀ (nM)		
		S	RBD	NTD		S	RBD	S2	SARS	MERS	OC43			
FD 10A	B	pos	-ve	-ve	pos	1.78	0.15	1.32	0.28	0.36	0.39	111.13		
FB 1E*	C	pos	-ve	-ve	pos	1.4	0.11	1.2	1.02	1.01	2.34	36		
FJ 4E*	B	pos	-ve	-ve	-ve	0.26	0.18	0.91	1.11	1.08	1.68	75.33		
EW 9C*	B	pos	-ve	-ve	pos	1.22	0.18	1.17	1.09	0.26	1.82	133.33		
FG 7A	A	pos	-ve	-ve	pos	0.28	0.17	1.05	0.14	0.13	0.16	133.33		
FM 1A	C	pos	-ve	-ve	-ve	0.25	0.17	0.88	0.17	0.09	0.14	133.33		
FB 9D*	C	pos	-ve	-ve	pos	1.43	0.12	1.27	1.28	1.5	2.13	-ve		
FD 1D	B	pos	-ve	-ve	pos	0.4	0.15	1.06	0.15	0.22	0.25	-ve		
FN 2C*	C	pos	-ve	-ve	pos	1.77	0.14	1.15	1.26	0.1	2.2	-ve		
Controls														
CR3022		pos	pos	-ve	pos	1.08	1.31	0.1	2.24	0.11	0.11	42	-ve	++
BS 1A (flu H3)		-ve	-ve	-ve	-ve	0.07	0.09	0.11	0.1	0.09	0.11	-ve	-ve	-ve

a The specificity of antibody was tested using flow cytometry with MDCK-SIAT1 cells expressing the spike glycoprotein, RBD and NTD. CR3022 is a SARS and SARS-CoV-2 RBD cross-reactive human MAb and BS-1A is an anti-influenza H3 human MAb.

b The antibody was assessed by immunofluorescence of wild-type SARS-CoV-2-infected Vero E6 cells.

c A sample (10 µg/ml) was considered positive when the measured extinction is at least 3 times the OD value of the negative control in the ELISA with SARS-CoV-2, SARS, MERS and OC43 spike proteins. CR3022 is an anti-SARS and SARS-CoV-2 RBD human MAb and BS-1A is an anti-influenza H3 human MAb. The OD value ≥ 1.00, 0.50–0.99, or ≤ 0.49 is highlighted in deep green, green and light green, respectively.

d The PRNT assay was performed with wild-type SARS-CoV-2 (see [methods](#)) and the 50% effective concentration (EC₅₀) was determined using linear regression analysis.

e ACE2-blocking activity of anti-RBD antibody compared to ACE2-Fc (see [methods](#)): +, partial; ++, IC₅₀ > ACE2-Fc; +++, IC₅₀ ~ = ACE2-Fc; +++++, IC₅₀ < ACE2-Fc.

* Memory phenotype.

Abbreviations: MAb, monoclonal antibody; FCM, flow cytometry; IFA, immunofluorescence; S, spike; RBD, receptor-binding domain; NTD, N-terminal domain; PRNT, plaque reduction neutralisation assay; ACE2, Angiotensin-Converting Enzyme 2.

<https://doi.org/10.1371/journal.ppat.1009352.t001>

IgG1, CR3022 and S309 human IgG1 antibodies [21,26]. These four control molecules have characterised binding footprints on the RBD defined by crystal structures [17,22,24,26], as does EY 6A [18]. Also included was the protease domain (residues 18–615) of ACE2 linked to the Fc region of human IgG1 (ACE2-Fc dimer).

The ten antibodies formed four cross-inhibiting clusters (Table 2), represented by antibodies EY 6A (cluster 1, equivalent to Class 4 of Barnes et al, which included CR3022 and VHH72), FI 3A (cluster 2, equivalent to Classes 1 and 2 of Barnes et al, which included H11-H4), FD 11A (cluster 3, equivalent to Class 3 of Barnes et al, which included S309) and FJ 10B (cluster 4, not represented in the Barnes classification) [20]. Cluster 2 is composed of antibodies in the Barnes Classes 1 and 2 that have overlapping binding footprints and cross inhibit each other's binding [20]. The strongest inhibitors of ACE2-Fc binding were in clusters 2 and 3 (Tables 1 and 2). Neutralising antibodies were detected in clusters 1, 2 and 3, with the strongest antibodies FI 3A and FD 11A being in clusters 2 and 3 (Tables 1 and 2). The sites of binding of the clusters of antibodies to the RBD and the ACE2 binding site are represented on a diagram of the RBD represented as in the shape of a squirrel, as an aide memoire for orientation in S8 Fig.

Neutralising antibodies targeting independent RBD epitopes and relationship to ACE2 blockade

Five neutralising anti-RBD MAbs partially or completely blocked the interaction between RBD and ACE2 (Tables 1 and 2, Fig 3). The most potent neutralising antibodies were ACE2 blockers (FI 3A in cluster 2, and FD 11A in cluster 3), and bound independently of each other to the RBD (Fig 3C). MAb EY 6A has been shown to alter the binding kinetics of the interaction without full inhibition [18] and it had a moderate effect on ACE2 binding in the assay where ACE2 was expressed at the cell surface. These three MAbs bound independently of each other indicating the existence of at least three neutralisation-sensitive epitopes within the RBD (Fig 3C).

All five neutralising MAbs to the RBD (EY 6A, FI 3A, FI 1C, FD 11A, FD 5A) had V gene sequences close to germline (S2 Table), indicating the development of *de novo* anti-RBD neutralising antibodies upon natural SARS-CoV-2 infection in humans.

The ability of convalescent sera to block soluble RBD for binding to cell-expressed ACE2 was assessed. Both convalescent sera from case A (D22) and case B (D26) exhibited detectable ACE2-blocking activities (Fig 3D). This serological activity is compatible with the isolation of potent ACE2-blocking antibodies from both patients (Table 1). By contrast, the D18 serum from case C showed minimal ACE2-blocking activity. Both cases A and B had prolonged fever and the development of pneumonia during hospitalization (S1 Table), which suggests that the development of ACE2-blocking antibody response in the convalescent stage is likely associated with clinical severity after infection.

Neutralising antibodies to S2

Six of nine MAbs specific for S2 showed moderate neutralisation in the PRNT assay (Table 1). The antibodies FB 1E, FJ 4E and EW 9C, are moderately neutralising (EC_{50} 36–133.33 nM), cross-react on the spike glycoprotein from the common cold betacoronavirus OC43, and show sequence characteristics of memory cells with high numbers of somatic mutations. This indicates that memory B cells, likely primed by an endemic or epidemic betacoronavirus related to OC43, can give rise to antibodies that neutralise SARS-CoV-2, albeit modestly. The other three neutralising antibodies specific for S2, FD 10A, FG 7A and FM 1A were close to germline in sequence (S2 Table) and did not cross-react strongly with other betacoronaviruses (Table 1).

Table 2. Competitive binding analysis of anti-SARS-CoV-2 RBD monoclonal antibodies^a.

MAB	Case	Vh	Neut ^b	Cluster	FI 4A-Bio	EY 6A-Bio	CR3022-Bio	VHH72-Fc-Bio	ACE2-Fc-Bio	FI 3A-Bio	FI 1C-Bio	HI1-H4-Fc-Bio	FD 5D-Bio	FD 11A-Bio	FJ 10B-Bio	EM 7B-Bio	EZ 7A-Bio
FI 4A	B	3-21	-	1	+	+	+	+	+	+	+	+	+	+	+	+	+
EY 6A	A	3-30	+	1	+	+	+	+	+	+	+	+	+	+	+	+	+
CR3022*			+	1	+	+	+	+	+	+	+	+	+	+	+	+	+
VHH72-Fc*			+	1	+	+	+	+	+	+	+	+	+	+	+	+	+
ACE2-Fc*			+		+	+	+	+	+	+	+	+	+	+	+	+	+
FI 3A	B	3-53	+	2	+	+	+	+	+	+	+	+	+	+	+	+	+
FI 1C	B	3-11	+	2	+	+	+	+	+	+	+	+	+	+	+	+	+
HI1-H4-Fc*			+	2	+	+	+	+	+	+	+	+	+	+	+	+	+
FN 12A	C	1-69	-	3	+	+	+	+	+	+	+	+	+	+	+	+	+
FD 5D	B	3-33	+	3	+	+	+	+	+	+	+	+	+	+	+	+	+
FD 11A	B	3-48	+	3	+	+	+	+	+	+	+	+	+	+	+	+	+
S309*			+	3	+	+	+	+	+	+	+	+	+	+	+	+	+
FJ 10B	B	5-10	-	4	+	+	+	+	+	+	+	+	+	+	+	+	+
FM 7B	C	1-3	-	4	+	+	+	+	+	+	+	+	+	+	+	+	+
EZ 7A	B	5-51	-	4	+	+	+	+	+	+	+	+	+	+	+	+	+
<i>-ve controls</i>																	
EW 8B (non-RBD-S1)			-		+	+	+	+	+	+	+	+	+	+	+	+	+
EW 9C (S2)			+		+	+	+	+	+	+	+	+	+	+	+	+	+
Z3B2 (flu stem)*			-		+	+	+	+	+	+	+	+	+	+	+	+	+

^a Competitive inhibition: values are shown for percentage inhibition and those with $\geq 75\%$ blocking, 50–74% blocking, and $< 50\%$ blocking are highlighted in red, orange and green, respectively.

^b Neutralisation of antibody against wild-type SARS-CoV-2 was analysed in the PRNT assay (+, positive; -, negative).

* SARS and SARS-CoV-2 cross-reactive anti-RBD MAb CR3022 and S309 were included as positive controls. SARS and SARS-CoV-2 cross-reactive anti-RBD nanobodies VHH72 and HI1-H4 were linked to the hinge and Fc region of human IgG1 and included as positive controls. ACE2-Fc was included as a positive control. Anti-SARS-CoV-2 non-RBD-S1 and S2 MAbs were included as negative controls. Anti-influenza MAb Z3B2 was included as a negative control.

Abbreviations: MAb, monoclonal antibody; Vh, heavy chain variable region; Neut, neutralization.

<https://doi.org/10.1371/journal.ppat.1009352.t002>

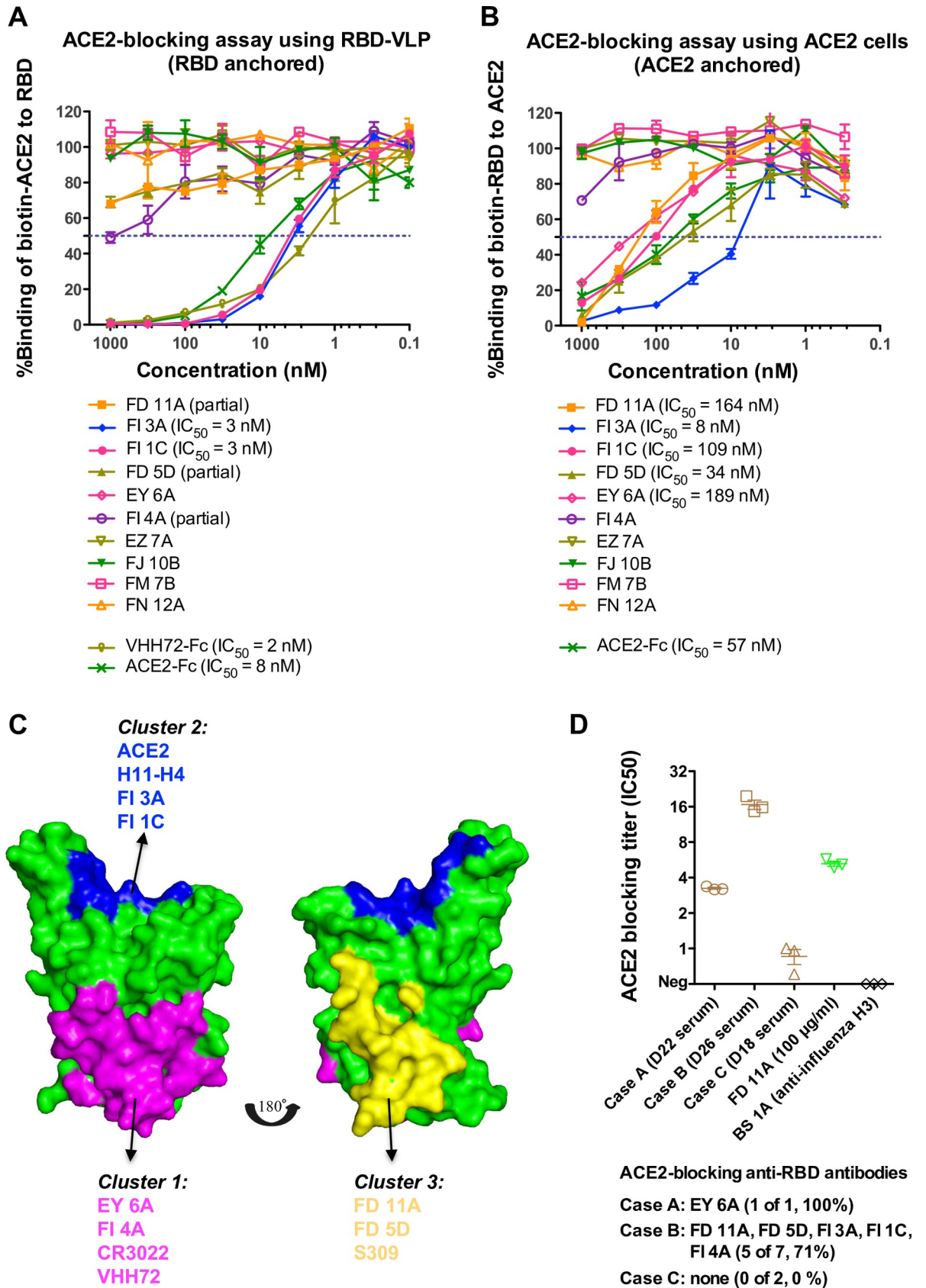


Fig 3. ACE2-blocking activities with anti-RBD antibodies and convalescent sera. The analyses were performed with (A) RBD anchored and (B) ACE2 anchored on plates (see [methods](#)). Anti-SARS-CoV-2 RBD nanobody VHH72 linked to the hinge and Fc region of human IgG1 and ACE2-Fc were included as controls. Experiments were performed in duplicate and repeated twice. (C) Mapping of neutralising anti-RBD antibodies on the SARS-CoV-2 RBD structure (PDB 6ZCZ) based on competitive binding and ACE2-blocking analyses. The RBD was coloured in green. The epitopes recognized by EY 6A, CR3022 and VHH72 (cluster 1 MAb) [18,21,24] were coloured in magenta. The epitopes recognized by H11-H4 (cluster 2 MAb) [17] were overlapping with ACE2-binding site and coloured in blue. The epitopes recognized by S309 (cluster 3 MAb) [26] were coloured in yellow. (D) Convalescent sera were analysed in the ACE2-blocking (ACE2 anchored) assay. Experiments were performed in triplicate. Anti-RBD antibody FD 11A and anti-influenza H3 antibody BS 1A were included as controls. Data are presented as mean \pm standard error of the mean. IC₅₀, 50% inhibitory concentration.

<https://doi.org/10.1371/journal.ppat.1009352.g003>

FD 10A exhibits the most potent neutralising activity in the PRNT assay and also completely inhibits SARS-CoV-2-induced cytopathic effect (see [methods](#)) at 8.33 nM.

Neutralising antibodies to non-RBD S1

Thirteen MAbs were defined that bound the S1 region and three, close to germline in sequence, were neutralising. FJ 1C showed neutralisation (EC₅₀ 55.5 nM), whilst FD 11E (EC₅₀ 70 nM) and FD 1E (EC₅₀ 110 nM) were moderately neutralising ([Table 1](#)). We investigated the specificity of these antibodies using flow cytometry and immunofluorescence with MDCK-SIAT1 cells expressing the NTD of spike glycoprotein linked to the transmembrane and cytoplasmic region of influenza haemagglutinin (see [methods](#)). FJ 1C (neutralising) and FD 7C bound strongly to this isolated NTD construct defining them as NTD-specific ([Table 1](#), [S9 Fig](#)).

Characterisation of anti-nucleocapsid antibodies

A set of 8 anti-SARS-CoV-2 nucleocapsid MAbs were derived from circulating plasmablasts in the naturally infected subjects ([Table 3](#), [S10 Fig](#)); 5 of these strongly cross-react with SARS

Table 3. The antigenic specificity and cross-reactivity of 8 anti-SARS-CoV-2 nucleocapsid monoclonal antibodies derived from COVID-19 patients.

MAb	Light chain isotype	Case	SARS-CoV-2 ^a	Cross-reactivity ^a		
				SARS	MERS	OC43
EY 2A*	Kappa	A	1.28	1.13	0.31	0.33
EY 3B*	Kappa	A	1.22	1.00	0.22	0.26
FD 6D*	Kappa	B	1.73	1.19	0.12	0.21
EZ 7B	Kappa	B	1.01	0.29	0.29	0.33
EZ 4A	Kappa	B	1.03	0.37	0.36	0.45
EZ 4C-1*	Kappa	B	0.60	0.47	0.26	0.33
EZ 11A	Lambda	B	1.29	1.31	0.16	0.13
FB 9B*	Lambda	C	1.27	1.28	0.13	0.21
Controls						
CR3022			0.07	0.06	0.07	0.17
BS 1A (flu H3)			0.08	0.07	0.07	0.15

^a A sample (10 μ g/ml) is considered positive when the measured extinction is at least 3 times the OD₄₅₀ value of the negative control in the ELISA. CR3022 is an anti-SARS RBD human MAb and BS-1A is an anti-influenza H3 human MAb. OD values of ≥ 1.00 or 0.50–0.99 or ≤ 0.49 are highlighted in deep orange, orange and light orange, respectively.

* Memory phenotype.

Abbreviations: MAb, monoclonal antibody.

<https://doi.org/10.1371/journal.ppat.1009352.t003>

CoV in ELISA. This suggested cross-reactivity of the antibody response to epitopes in nucleocapsids of betacoronaviruses following natural infection with SARS-CoV-2.

The 8 MAbs were evolved from 7 clonal groups defined by their heavy chain VDJ and light chain VJ rearrangements (S3 Table). Those cross-reactive with SARS-CoV carried more nucleotide and amino acid substitutions than SARS-CoV-2-specific MAbs in their variable domains, but this trend did not reach statistical significance (Cross-reactive heavy 24 ± 19 nt versus specific heavy 8 ± 14 nt, $p = 0.45$; Cross-reactive heavy 13 ± 10 aa versus specific heavy 5 ± 8 aa, $p = 0.45$; two-tailed Mann-Whitney test; Fig 2D).

Discussion

We detected a robust and rapid plasmablast response encoding diverse anti-spike glycoprotein and anti-nucleocapsid antibody populations within 3 weeks of onset of illness in COVID-19 patients. The concomitant serologic response occurred as early as the first week after illness onset, with gradually increasing levels of SARS-CoV-2 spike glycoprotein- and RBD-binding IgG antibodies from the second to third week after symptom onset. The kinetics of plasmablast and virus-specific serologic responses was observed to vary between subjects. Consecutive samples from donor B showed a highly expanded plasmablast subset at the time of progression into pneumonia, followed by class-switching to an IgG-predominant plasmablast response until week three of illness. On the other hand, donor C presented with mild symptoms and produced an early plasmablast response with class-switching at the end of first week of symptom onset. Thevarajan et al demonstrated a similar kinetic of B cell response in a mild COVID-19 case, in whom the peripheral plasmablast response and the SARS-CoV-2-binding IgG antibodies peaked at day eight, soon after the disappearance of fever [8]. An early class-switching phenotype of the humoral response was also noted within the first week of onset in paediatric patients who mainly experienced mild illness after SARS-CoV-2 infection, although the immunological basis for this phenotype is unclear [27]. Both peak plasmablast frequency and serologic titre for spike glycoprotein were higher in donor B, who presented with severe symptoms, than in donor C. Similar observations on the serologic titre and clinical severity have been reported by others [10]. Such plasmablast response may originate from naïve or memory B cells, although its fate remains largely undetermined in humans [28,29]. The IgG spike-specific plasmablasts that are detectable as soon as at the end of first week and become dominant after the second week of onset are further characterised in the study and these cells may represent either a rapid class-switching in the germinal center or a recall memory [30–32].

In this study, a substantial subset of plasmablast-derived anti-S2 (five of nine, 56%) cross-reacted with human betacoronavirus OC43. Cross-reactivity among betacoronaviruses has also been reported in polyclonal sera [12–14]. Human coronavirus OC43, discovered in the 1960s, is one of the major betacoronaviruses that cause common colds in the community [33,34], and severe respiratory infections in elderly and immunocompromised individuals [12,35]. Epidemiologic surveys reveal that OC43 infection can occur in early childhood, and that OC43 seropositivity reaches nearly 90% in adults [36,37]. The S2 component of SARS-CoV-2 spike glycoprotein shares 43~89% amino acid identity with SARS, MERS and OC43, and, similarly, the amino acid sequence of SARS-CoV-2 nucleocapsid protein of is 34~90% homologous to those of other betacoronaviruses (S11 Fig and S12 Fig), suggesting the presence of conserved epitopes on these antigens.

The presence of pre-existing immune memory to betacoronavirus that cross-react with SARS-CoV-2 is supported by the accumulation of somatic mutations in the genes encoding cross-reactive antibodies isolated from COVID-19 patients (Fig 2C, S2 Table). This situation is

reminiscent of re-exposure to immunogenic epitopes shared by closely related viruses leading to induction of broadly cross-reactive antibodies in patients infected with influenza, dengue or Zika viruses [38–40].

The 32 MAbs that bound to the spike glycoprotein were systematically tested for neutralisation (summarised in Table 1). Results established that neutralising epitopes were present on the RBD, S1-NTD, S1-non NTD/RBD, and S2 regions of the spike glycoprotein. The range of neutralisation EC_{50} titres against live SARS-CoV-2 reported in the literature for human and murine monoclonal antibodies span at least three orders of magnitude, from ng/ml to μ g/ml [41,42]. Our results reflect the range of values in *in vitro* potency. The relationship between the EC_{50} value in neutralisation assays and therapeutic potential is not established, although antibodies to the RBD with EC_{50} in the nanogram range have shown therapeutic activity in small animal models [43–45]. The majority of the most strongly neutralising antibodies were close to germline in sequence, showing that full affinity maturation is not required in order to achieve SARS-CoV-2 virus neutralisation. We made a similar observation for antibodies induced by an Ebola vaccine [25], and this has been observed in other collections of monoclonal antibodies to SARS-CoV-2 [7,42–49].

The RBDs of SARS and SARS-CoV-2 are known to contain neutralising epitopes [18,41–51], and vaccines based on the RBD of SARS and SARS-CoV-2 induce strong neutralising antibodies that are protective in animal models [52–54]. There is a tendency for the most potent neutralising antibodies to be those that block the binding of the RBD to its receptor ACE2 [41–51,55–57]. Previous structural studies demonstrated that potent antibodies with footprints overlapping that of ACE2 are composed of two major subgroups (named Class 1 and Class 2 by Barnes et al) [20], one with representative Vh3-53 gene usage and short CDR3 binding to the RBD in an up conformation and the other binding RBDs in both up and down conformations and even adjacent RBDs [20,58]. Potent MAb FI 3A shares similar characteristics with the first subgroup described above. Occasional antibodies that do not occupy the ACE2 footprint or weakly block ACE2 binding, i.e., S309, FD 11A and EY 6A, can be almost as potent, perhaps through spike trimer cross-linking or triggering a conformational change in the spike glycoprotein that renders it non-functional [7,18,26,49].

We characterise MAbs targeting the RBD that can be arranged into four cross-inhibiting clusters (Table 2). Three of these MAb clusters (represented by EY 6A, FI 3A and FD 11A) demonstrate neutralisation of SARS-CoV-2 to some level, while those in the fourth (represented by FM 7B) did not neutralise. This suggests that three neutralising antibodies may be able to bind to the RBD simultaneously. The most potent neutralising MAbs fall in two clusters and interfere strongly with ACE2 binding, which may be exploited therapeutically. For instance, antibodies FI 3A in cluster 2 (EC_{50} 8.67 nM) and FD 11A in cluster 3 (EC_{50} 0.05 nM) could be combined to limit possible selection of neutralisation-resistant variants. This principle has been demonstrated in recent studies [45,47,59].

Neutralisation by human MAbs to the S1-NTD of SARS-CoV-2 has been described [44,60], but their mechanism of action is not known. The range of neutralising EC_{50} titres (0.09–51.1 nM) was overlapping with those targeting the RBD, similar to our NTD-specific antibody FJ 1C. Cocktails of antibodies that include a representative to the NTD would further reduce the likelihood of selecting neutralisation-resistant viruses. A second strong binder to the NTD, FD 7C, was not neutralising. Structural comparisons of these two antibodies bound to spike glycoprotein may provide insight into the neutralising action of FJ 1C [60].

We detected a subset of six MAbs to the S2 region of the spike glycoprotein that neutralised moderately (EC_{50} 36–133 nM). Similar results are found in the antibodies to SARS [61–63]. It has been shown that the neutralizing activity of anti-SARS S2 antibody involves the inhibition of membrane fusion, but the function of anti-SARS-CoV-2 S2 antibodies could be complex

and remain undetermined yet [61–65]. Five of our anti-S2 antibodies were clearly derived from a memory population; showing significant accumulation of somatic mutations in the MAb encoding genes and cross-reactivity for the OC43 common cold virus spike glycoprotein (Fig 2C). Further investigation is required to ascertain whether such antibodies, that may be weak- or non-neutralising and cross-reactive with common cold viruses, are beneficial or detrimental with respect to COVID-19 disease. Recent evidence is not conclusive on this issue [66,67].

Our results have significance for serologic tests employing the N and S2 antigens of SARS-CoV-2. Serologic surveys, some of which are based on these antigens, with sera from donors infected with SARS-CoV-2 during the spring and summer months have shown very high specificity (as judged by comparing convalescent sera from COVID-19 patients versus sera collected in the pre-COVID-19 period) (www.gov.uk/government/publications/covid-19-laboratory-evaluations-of-serological-assays). However, if many individuals have memory B cells to the S2 antigen of circulating betacoronaviruses that cross-react with SARS-CoV-2, concurrent winter infections with these viruses might erode the specificity of serologic tests for SARS-CoV-2 that include the S2 antigen. Cross-reactivity of antibodies targeting the S1 subunit or RBD is relatively much lower, so using this antigen is more likely to give a true indication of SARS-CoV-2 specificity.

In summary, COVID-19 patients developed strong anti-SARS-CoV-2 spike glycoprotein and nucleocapsid plasmablast and antibody responses. A panel of IgG MAbs targeted a diverse spectrum of epitopes on the RBD, S1-NTD, non-NTD/RBD S1 and S2 regions of the spike glycoprotein, of which 14 neutralised wild-type viruses with EC_{50} s in the range 0.05 to ~133 nM. Neutralising activities of the majority of anti-RBD MAbs were linked to ACE2-binding blockade, and non-competing pairs of such MAbs, perhaps combined with a neutralising MAb to the NTD, offer potential formulations for the development of prophylactic and therapeutic agents against SARS-CoV-2. Antibody responses to the S2 component of spike glycoprotein confirm cross-reactivity with a common cold virus.

Methods

Ethics statement

The study protocol and informed consent were approved by the ethics committee at the Chang Gung Medical Foundation and the Taoyuan General Hospital, Ministry of Health and Welfare. Written informed consent was received from each participant prior to inclusion in the study. The study and all associated methods were carried out in accordance with the approved protocol, the Declaration of Helsinki and Good Clinical Practice guidelines.

Study subjects

This study was designed to isolate SARS-CoV-2 antigen-specific MAbs from peripheral plasmablasts of humans infected with SARS-CoV-2 and to characterise the antigenic specificity and phenotypic activities of the MAbs. Diagnosis of SARS-CoV-2 infection was based on positive real-time reverse transcriptase polymerase chain reaction results of respiratory samples.

Staining and sorting of plasmablasts

Freshly separated peripheral blood mononuclear cells (PBMCs) or thawed PBMCs were stained with fluorescent-labelled antibodies to cell surface markers purchased from BD Biosciences, USA; Pacific blue anti-CD3 (clone UCHT1, Cat. No. 558117, BD), Fluorescein isothiocyanate anti-CD19 (clone HIB19, Cat. No. 555412, BD), Phycoerythrin-Cy7 anti-CD27 (clone

M-T271, Cat. No. 560609, BD), Allophycocyanin-H7 anti-CD20 (clone L27, Cat. No. 641396, BD), Phycoerythrin-Cy5 anti-CD38 (clone HIT2, Cat. No. 555461, BD) and Phycoerythrin anti-human IgG (clone G18-145, Cat. No. 555787, BD). The CD3^{neg}CD19^{pos}CD20^{neg}CD27^{hi}CD38^{hi}IgG^{pos} plasmablasts were gated and isolated in chamber as single cells as previously described [32].

Production of human IgG 1 monoclonal antibodies

Sorted single cells were used to produce human IgG MAb as previously described [32]. Briefly, the variable region genes from each single cell were amplified in a reverse transcriptase polymerase chain reaction (RT-PCR: QIAGEN, Germany) using a cocktail of sense primers specific for the leader region and antisense primers to the C γ constant region for heavy chain and C κ and C λ for light chain. The RT-PCR products were amplified in separate polymerase chain reactions for the individual heavy and light chain gene families using nested primers to incorporate restriction sites at the ends of the variable gene as previously described [32]. These variable genes were then cloned into expression vectors for the heavy and light chains. Plasmids were transfected into the HEK293T cell line for expression of recombinant full-length human IgG MAb in serum-free transfection medium. A selected panel of MAb were further expanded and purified.

To determine the individual gene segments employed by VDJ and VJ rearrangements and the number of nucleotide mutations and amino acid replacements, the variable domain sequences were aligned with germline gene segments using the international ImmMunoGeneT-ics (IMGT) alignment tool (http://www.imgt.org/IMGT_vquest/input).

Enzyme-linked immunosorbent assay (ELISA)

ELISA plates (Corning 96-well Clear Polystyrene High Bind Stripwell Microplate, USA) were coated with 8 μ g/ml SARS-CoV-2 antigens (spike glycoprotein extracellular or receptor-binding domains or S2 subunit, or nucleocapsid) or SARS antigen (spike glycoprotein S1 or S2 subunit, or nucleocapsid) or MERS antigen (spike glycoprotein extracellular domain, or nucleocapsid) or human coronavirus OC43 antigen (spike glycoprotein extracellular domain, or nucleocapsid) at 4°C overnight. Recombinant SARS-CoV-2 proteins were purchased from Sino Biologicals (S1+S2 extracellular domain, 40589-V08B1; RBD, 40592-V08B; S2, 40590-V08B; Nucleocapsid, 40588-V08B) and were produced in the baculovirus-insect cell expression system. Recombinant SARS proteins were purchased from Sino Biologicals (S1, 40150-V08B1; S2, 40150-V08B3; Nucleocapsid, 40143-V08B) and were produced in the baculovirus-insect cell expression system. Recombinant MERS proteins were purchased from Sino Biologicals (S1+S2 extracellular domain, 40069-V08B; Nucleocapsid, 40068-V08B) and were produced in the baculovirus-insect cell expression system. Recombinant coronavirus OC43 proteins were purchased from Sino Biologicals (S1+S2 extracellular domain, 40607-V08B; Nucleocapsid, 40643-V07E). Plates were washed with phosphate-buffered saline containing 0.05% Tween-20 and blocked with 3% bovine serum albumin (BSA) at room temperature for 1 hour on a shaker. Serial dilutions of MAb-containing cell culture supernatant or purified MAb were added and plates were incubated at 37°C for 1 hour. Plates were washed and incubated with horseradish peroxidase-conjugated rabbit anti-human IgG secondary antibody (Rockland Immunochemicals, USA). Plates were washed and developed with TMB substrate reagent (BD Biosciences, USA). Reactions were stopped with 0.5M hydrochloric acid and absorbances was measured at 450nm on a microplate reader. Non-transfected cell culture supernatant, anti-influenza H3 human IgG MAb BS 1A (in house), anti-SARS spike glycoprotein MAb CR3022 and convalescent serum were used as controls for each experiment.

Reaction yielding an absorbance value above three times the mean absorbance of the negative control BS 1A were considered positive.

Flow-cytometry based binding assay

MDCK-Spike cells were produced by stably transducing parental MDCK-SIAT1 cells with cDNA expressing full-length SARS-CoV-2 spike glycoprotein. MDCK-RBD cells were produced by, stably transducing MDCK-SIAT1 cells [32] with a Lentiviral vector encoding a cDNA expressing RBD amino acids 340–538 (NITNLCPFGEVFNATRFASVYAWNRRKRI SNCVADYSVLYNSASFSTFKCYGVSPTKLNDLCFTNVYADSFVIRGDEVQRQIAPGQTGKI ADYNYKLPDDFTGCVIAWNSNNLDSKVGGNYNLYRLFRKSNLKPFRDISTEIYQAG STPCNGVEGFNCYFPLQSYGFQPTNGVGYQPYRVVLSFELLHAPATVCGPKK) fused via a short linker to the transmembrane domain of haemagglutinin H7 (A/Hong Kong/125/2017) (EPI977395) at the C-terminus for surface expression. MDCK-NTD cells were produced by stably transfecting parental MDCK-SIAT1 cells [32] with cDNA expressing the SARS-CoV-2 NTD amino acids (VNLTTRTQLPPAYTNSFTRGVYYPDKVFRSSVLHSTQDLFLPFFSN VTWFHAIHVSGTNGTKRFDNPVLPFNDGVYFASTEKSNIIRGWIFGTTLDSTQSLIVN NATNVVIKVCFCNDPFLGVYYHKNNKSWMESEFRVYSSANNCTFEYVSQPFLMDL EGKQGNFKNLREFVFKNIDGYFKIYSKHTPINLVRDLQPQFSALEPLVDLPIGINITRFQTL LALHRSYLTPGDSSSGWTAGAAAYYVGYLQPRTFLLKYNENGTITDAVDCALDPLSET KCTLKS) fused to the transmembrane domain of haemagglutinin H7 (A/Hong Kong/125/2017) (EPI977395) at the C-terminus for surface expression. MDCK-Spike, MDCK-RBD and MDCK-NTD cells were then FACS sorted for highly expressing cells using the CR3022 or FD7C antibody. MDCK-Spike or MDCK-RBD or MDCK-NTD cells were prepared and resuspended. Cells were probed with purified MAbs in 3% BSA. Bound primary antibodies were detected with FITC-conjugated anti-IgG secondary. The binding activities were analysed by BD FACSCanto II flow cytometer (BD Biosciences, USA).

Immunofluorescence assay

Under biosafety level 3 (BSL-3) conditions, Vero E6 cells were infected with 100 TCID₅₀ (median tissue culture infectious dose) SARS-CoV-2 (hCoV-19/Taiwan/CGMH-CGU-01/2020, EPI_ISL_411915). Infected cells were placed on coverslips and, and fixed with acetone at room temperature for 10 minutes. After blocking with 1% BSA at room temperature for 1 hour and washing, fixed cells were incubated with MAb-containing cell culture supernatant. The anti-influenza human monoclonal antibody BS 1A, anti-SARS spike glycoprotein MAb CR3022 and convalescent serum were used as antibody controls for each experiment. Following incubation and wash, cells were stained with FITC-conjugated anti-human IgG secondary antibody and Evans blue dye as counterstain. Antibody-bound infected cells demonstrated an apple-green fluorescence against a background of red fluorescing material stained by the Evans Blue counterstain. Images were acquired with original magnification 40x, scale bar 20 μm.

Plaque reduction neutralisation assay

Confluent monolayers of Vero E6 cells in 96-well plates were incubated with ~14 plaque forming units (PFU) of SARS CoV-2 (hCoV-19/England/02/2020, EPI_ISL_407073) and antibodies in a 2-fold dilution series (triplicates) for 3 hours at room temperature. Inoculum was then removed, and cells were overlaid with plaque assay overlay. Cells were incubated at 37°C, 5% CO₂ for 24 hours prior to fixation with 4% paraformaldehyde at 4°C for 30 minutes. Fixed cells were then permeabilised with 0.2% Triton-X-100 and stained with a horseradish

peroxidase conjugated-antibody against virus protein for 1 hour at room temperature. TMB substrate was then added to visualise virus plaques as described previously for influenza virus [68]. Convalescent serum from COVID-19 patients was used as a control.

Fluorescent focus-forming units microneutralisation assay (FMNT)

In brief, this rapid, high-throughput assay determines the concentration of antibody that produces a 50% reduction in infectious focus-forming units of authentic SARS-CoV-2 in Vero cells, as follows. Triplicate serial dilutions of antibody are pre-incubated with a fixed dose of SARS-CoV-2 (Australia/VIC01/2020, GenBank MT007544) [69] in triplicate before incubation with Vero cells. A carboxymethyl cellulose-containing overlay is used to prevent satellite focus formation. Twenty hours post-infection, the monolayers are fixed with paraformaldehyde and stained for N antigen using MAb EY 2A. After development with a peroxidase-conjugated antibody and substrate, foci are enumerated by enzyme-linked immune absorbent spot reader. Data are analysed using four-parameter logistic regression (Hill equation) in GraphPad Prism 8.3.

Quantitative PCR-based neutralisation assay

Neutralisation activity of MAb-containing supernatant was measured using SARS-CoV-2 (hCoV-19/Taiwan/CGMH-CGU-01/2020, EPI_ISL_411915) infected Vero E6 cells. Briefly, Vero E6 cells were pre-seeded in a 96 well plate at a concentration of 10^4 cells per well. The following day, MAb-containing supernatants were mixed with equal volumes of 100 TCID₅₀ virus preparation and incubated at 37°C for 1 hour, then mixtures were added to seeded Vero E6 cells and incubated at 37°C for 5 days. Cell, virus and virus back-titration controls were setup for each experiment. At day 5 the culture supernatant was harvested from each well, and virus RNA was extracted and quantified by real-time RT-PCR targeting the E gene of SARS-CoV-2 as previously described. The cycle threshold values of real-time RT-PCR were used as indicators of the copy number of SARS-CoV-2 RNA in samples with lower cycle threshold values corresponding to higher virus copy numbers.

CPE-based neutralisation assay

Vero E6 cells in Dulbecco's Modified Eagle's Medium containing 10% FBS were added into 96-well plates and incubated at 37°C with 5% CO₂ overnight to reach confluence. After washing with virus growth medium (VGM: Dulbecco's Modified Eagle's Medium containing 2% FBS), two-fold serially diluted MAbs in VGM starting at 100 µg/ml were added to each duplicated well. The plates were immediately transferred to a BSL-3 laboratory and 100 TCID₅₀ SARS-CoV-2 (hCoV-19/Taiwan/4/2020, EPI_ISL_411927) in VGM was added. The plates were further incubated at 37°C with 5% CO₂ for three days and the cytopathic morphology of the cells was recorded using an ImageXpress Nano Automated Cellular Imaging System.

Competitive binding assays

Competitive binding assays were performed as described previously [25] with slight modifications for epitope mapping of the anti-RBD MAbs. Briefly, 0.5 µg/ml of RBD-VLP were coated on NUNC plates (50 µl per well) overnight at 4°C, washed and blocked with 300 µl of 5% (w/v) dried skimmed milk in PBS for 1 hour at room temperature prior to the assays. Antibody was biotinylated using EZ-Link Sulfo-NHS-LC-biotin (21237; Life Technologies) and then mixed with competing MAb (in at least 10-fold excess) and transferred to the blocked NUNC plates

for 1 hour. A second layer Streptavidin-HRP (S911, Life Technologies) diluted 1:1,600 in PBS/0.1% BSA (37525; Thermo Fisher Scientific) was then added and incubated for another 1 hour. Plates were then washed, and signal was developed by adding POD substrate (11484281001, Roche) for 5 minutes before stopping the reaction with 1 M H₂SO₄. Absorbance (OD₄₅₀) was measured using a Clariostar plate reader (BMG, Labtech). Mean and 95% confidence interval of 4 replicate measurements were calculated. Competition was measured as: $(X - \text{minimum binding}) / (\text{maximum binding} - \text{minimum binding})$, where X is the binding of the biotinylated MAb in the presence of competing MAb. Minimum binding is the self-blocking of the biotinylated MAb or background binding. Maximum binding is binding of biotinylated MAb in the presence of non-competing MAb (anti-influenza N1 neuraminidase MAb).

ACE2 blocking assays

Two assays were used to determine the blocking of binding of ACE2 to RBD by MAbs. RBD was anchored on the plate in the first assay whereas ACE2 was anchored for the second assay.

In the first ACE2 blocking assay, RBD-VLP (Spycatcher-mi3 VLP-particles conjugated with Spytagged-RBD recombinant protein) [19] was coated on ELISA plates as described for the competitive binding assay. Recombinant ACE2-Fc (18–615) protein expressed in Expi293F (Life Technologies) cells was chemically biotinylated using EZ-link Sulfo-NHS-Biotin (A39256; Life Technologies) and buffer exchanged to PBS using a Zebaspin desalting column (Thermo Fischer). MAbs were titrated in duplicate or triplicate as half-log serial dilution, 8-point series starting at 1 μM in 30 μl volume with PBS/0.1% BSA buffer. 30 μl of biotinylated ACE2-Fc at approx. 0.2 nM (40 ng/ml) was added to the antibodies. 50 μl of the mixture was transferred to the PBS-washed RBD-VLP coated plates and incubated for 1 hour at room temperature. Secondary Streptavidin-HRP antibody (S911, Life Technologies) diluted to 1:1600 was then added to the PBS-washed plates and incubated for 1 h at room temperature. Plates were then washed four times with PBS and signal was developed by adding POD substrate (11484281001, Roche) for 5 minutes before stopping with 1 M H₂SO₄. OD₄₅₀ was measured using a Clariostar plate reader (BMG, Labtech). The control antibody (a non-blocking anti-influenza N1 MAb) or ACE2-Fc without antibody used to obtain the maximum signal and wells with PBS/BSA buffer only were used to determine the minimum signal. Graphs were plotted as % binding of biotinylated ACE2 to RBD. $\text{Binding \%} = \{(X - \text{Min}) / (\text{Max} - \text{Min})\} * 100$ where X = measurement of the antibody, Min = buffer only, Max = biotinylated ACE2-Fc alone. 50% inhibitory concentrations of the antibodies against ACE2 were determined using non-linear regression curve fit using GraphPad Prism 8.

The second ACE2 blocking assay was performed as described previously [17,18]. Briefly, MDCK-SIAT1 cells were stably transfected to overexpress codon-optimised human ACE2 cDNA (NM_021804.1) using lentiviral vector and FACS sorted (MDCK-ACE2). Cells (3×10^4 per well) were seeded on a flat-bottomed 96-well plate the day before the assay. RBD-6H (340–538; NITN.GPKK) was chemically biotinylated using EZ-link Sulfo-NHS-Biotin (A39256; Life Technologies). Serial half-log dilutions (starting at 1 μM) of antibodies and controls were performed in a U-bottomed 96 well plate in 30 μl volume. 30 μl of biotinylated RBD (25 nM) were mixed and 50 μl of the mixture was then transferred to the MDCK-ACE2 cells. After 1 hour a second layer Streptavidin-HRP antibody (S911, Life Technologies) diluted 1:1,600 in PBS/0.1% BSA (37525; Thermo Fisher Scientific) was added and incubated for another 1 hour. Plates were then washed four times with PBS and signal was developed by adding POD substrate (11484281001, Roche) before stopping with 1 M H₂SO₄ after 5 minutes. OD₄₅₀ was measured using a Clariostar plate reader (BMG, Labtech). The control antibody (a non-blocking anti-influenza N1 antibody) was used to obtain maximum signal and PBS only wells were

used to determine background. Graphs were plotted as % binding of biotinylated RBD to ACE2. The 50% inhibitory concentration of the blocking antibody was determined as described above.

Statistics

The two-tailed Mann-Whitney test was performed to compare differences between two independent groups. The 50% effective concentration (EC₅₀) was determined using linear regression analysis. A p value of less than 0.05 was considered significant. Graphs were presented by Microsoft Excel and GraphPad Prism software.

Supporting information

S1 Table. Clinical characteristics of COVID-19 patients and sampling dates in the study.
(DOC)

S2 Table. Anti-SARS-CoV-2 spike monoclonal antibody heavy and light chain variable domain gene usage.
(DOC)

S3 Table. Anti-SARS-CoV-2 nucleocapsid monoclonal antibody heavy and light chain variable domain gene usage.
(DOC)

S1 Fig. Binding of anti-spike antibodies to SARS-CoV-2-infected cells in immunofluorescence assay. Representative immunofluorescence staining of anti-RBD, anti-S1 and anti-S2 MAbs are shown as apple-green fluorescence a background of red fluorescing material stained by Evans Blue counterstain. Anti-influenza H3 MAb BS 1A was included as a control. Images were acquired with original magnification 40x, scale bar 20 μ m.
(TIF)

S2 Fig. The binding activity of anti-SARS-CoV-2 S2 antibodies with spike-expressed MDCK cells in the flow cytometry. We produced MDCK-Spike by stably transducing parental MDCK-SIAT1 cells with cDNA expressing full-length SARS-CoV-2 spike glycoprotein. This cell membrane-bound full-length spike carries trimer-stabilizing proline mutations (986KV987 to 986PP987) and substitutions at the S1-S2 furin cleavage site (682RRAR685 to 682GSAG685), which indicates that the spike would display the prefusion conformation. MDCK-H3 cells were stained in the control experiment. Anti-influenza H3 MAb BS-1A was included as an antibody control. Each experiment was repeated twice (n = 2). The binding percentage was presented as mean \pm standard error of the mean.
(TIF)

S3 Fig. Binding activity of anti-SARS-CoV-2 RBD antibodies to MDCK-RBD cells measured by flow cytometry. Anti-influenza H3 MAb BS-1A was included as a control. Binding percentages are presented as mean \pm standard error of the mean. Each experiment was repeated twice (n = 2). The 50% binding concentration (BC₅₀) was measured with a curve fit using non-linear regression.
(TIF)

S4 Fig. The correlation of CDR3 length with BC₅₀ among anti-RBD antibodies. The CDR3 length (number of amino acids) and MAb gene mutation numbers are presented as mean \pm standard error of the mean (< 0.5 μ g/ml, n = 5 versus > 0.5 μ g/ml, n = 5). The two-tailed Mann-Whitney test was performed to compare the CDR3 length and mutation numbers

between two groups. * $P < 0.05$; ns, non-significant; BC_{50} , 50% binding concentration. (TIF)

S5 Fig. Neutralisation of wild-type SARS-CoV-2 by anti-RBD monoclonal antibodies. Neutralisation assays were performed on the indicated antibodies according to the fluorescent focus-forming units microneutralisation method (see [methods](#)). Data were normalized to control (no antibody) values of foci, and the grey region comprises ± 1 standard deviation the mean control values. Individual points are displayed ± 1 standard deviation of technical, and curves are shown only where the data for a particular antibody fitted the standard dose-response (Hill) equation ($n = 3$). Partial: MAb neutralises at least $\sim 40\%$ viruses at 100 nM (highest concentration tested). EC_{50} , 50% effective concentration. (TIF)

S6 Fig. Neutralisation of SARS-CoV-2 by monoclonal antibodies in the PCR-based neutralisation assay. (A) An illustrative example of measuring Ct value of virus signal in the tissue-culture supernatant of SARS-CoV-2 infected Vero E6 cells using an E gene-based real-time reverse-transcription PCR assay. The right shift of the amplification plot reflects the increase in Ct value and the decrease of viral load. (B) Neutralisation data for MAbs EW 9C, EY 6A, FD 5D, FD 11A and FI 3A. Increases in Ct value indicate decreases in virus loads. Each unit increase indicates a 2x reduction resulting from the presence of MAb. A 10x increase in Ct = 1,024-fold reduction of virus load. (TIF)

S7 Fig. Binding of ACE2-Fc and MAbs to ST1-RBD (340–538) compared to ST1-RBD-mi3VLP in the ELISA. RBD bound directly to plate (Panel 1) fails to bind ACE2-Fc, but RBD-VLP bound to plate (Panel 2) exposes the ACE2 binding site on RBD, and the epitopes bound by the MAbs CR3022 and EY 6A. VLP only (Panel 3) was included as a control in the assay. Other MAbs EW 9B, EW 9C, EW 8B bind elsewhere on the spike glycoprotein (therefore are negative in this assay), anti-influenza H7 haemagglutinin MAb is a negative control. Each experiment was repeated twice. (TIF)

S8 Fig. The binding site of the clusters of anti-RBD antibodies are represented on a “squirrel” diagram of the RBD. Cluster 2 antibodies is composed of antibodies in the Barnes Classes 1 and 2 antibodies that bind to the left and right side of the head/shoulder of the “squirrel” RBD [20]. Cluster 1 antibodies that correspond to Barnes Class 4 antibodies bind to the left hip of the “squirrel” RBD. Cluster 3 antibodies that correspond to Barnes Class 3 antibodies bind to the right hip of the “squirrel” RBD. (TIF)

S9 Fig. The binding activity of anti-SARS-CoV-2 NTD with MDCK-NTD cells in immunofluorescence. Anti-influenza neuraminidase Z3-B2 (Flu MAb) was included as control in the experiment. Each experiment was repeated twice. Values are presented as mean \pm standard error of the mean. (TIF)

S10 Fig. The binding activity of anti-SARS-CoV-2 nucleocapsid (N) antibodies with antigens of SARS-CoV-2 in ELISA. Anti-influenza H3 BS-1A and anti-SARS spike CR3022 MAbs were included as controls. Each experiment was repeated twice. OD450 values are presented as mean \pm standard error of the mean. (TIF)

S11 Fig. Percentage identities of spike glycoprotein, RBD and S2 amino acid residues among human coronaviruses. Sequences were retrieved from the Genbank database (DQ243979, DQ243983, KY014282, KF963239, L14643, KF600651, KJ556336, AY291451, AY463060) and the EpiFlu database of GISAID (EPI_ISL_411915, EPI_ISL_424972, EPI_ISL_424973, EPI_ISL_444278).
(TIF)

S12 Fig. Percentage identities of nucleocapsid amino acid residues among human coronaviruses. Sequences were retrieved from the Genbank database (DQ243957, KM055524, KY014282, KF963212, KF600651, KJ556336, AY291451, AY463060) and the EpiFlu database of GISAID (EPI_ISL_411915, EPI_ISL_424972, EPI_ISL_424973, EPI_ISL_444278).
(TIF)

Acknowledgments

We acknowledge the BD FACSAria cell sorter service provided by the Core Instrument Center of Chang Gung University. We would like to acknowledge Paul Sopp and Craig Waugh in the flow cytometry facility at the MRC WIMM for providing cell sorting services.

Author Contributions

Conceptualization: Kuan-Ying A. Huang.

Data curation: Kuan-Ying A. Huang, Tiong Kit Tan, Lisa Schimanski, William James, Rodney S. Daniels, John W. McCauley, Pramila Rijal, Alain R. Townsend.

Formal analysis: Kuan-Ying A. Huang, Tiong Kit Tan, Ting-Hua Chen, Chung-Guei Huang, Lisa Schimanski, Che Ma, William James, Rodney S. Daniels, John W. McCauley, Pramila Rijal, Alain R. Townsend.

Funding acquisition: Kuan-Ying A. Huang, Alain R. Townsend.

Investigation: Kuan-Ying A. Huang, Alain R. Townsend.

Methodology: Kuan-Ying A. Huang, Ruth Harvey, Saira Hussain, Cheng-Pin Chen, Adam Harding, Javier Gilbert-Jaramillo, Xu Liu, Michael Knight, Shin-Ru Shih, Yi-Chun Lin, Chien-Yu Cheng, Shu-Hsing Cheng, Yhu-Chering Huang, Tzou-Yien Lin, Jia-Tsong Jan, Che Ma, William James, Rodney S. Daniels, John W. McCauley, Pramila Rijal, Alain R. Townsend.

Project administration: Kuan-Ying A. Huang, Alain R. Townsend.

Resources: Kuan-Ying A. Huang, Alain R. Townsend.

Software: Kuan-Ying A. Huang, Alain R. Townsend.

Supervision: Kuan-Ying A. Huang, Alain R. Townsend.

Validation: Kuan-Ying A. Huang, Alain R. Townsend.

Visualization: Kuan-Ying A. Huang, Tiong Kit Tan, Pramila Rijal, Alain R. Townsend.

Writing – original draft: Kuan-Ying A. Huang, Tiong Kit Tan, William James, Rodney S. Daniels, John W. McCauley, Pramila Rijal, Alain R. Townsend.

Writing – review & editing: Kuan-Ying A. Huang, Tiong Kit Tan, Ting-Hua Chen, Chung-Guei Huang, Ruth Harvey, Saira Hussain, Cheng-Pin Chen, Adam Harding, Javier Gilbert-Jaramillo, Xu Liu, Michael Knight, Lisa Schimanski, Shin-Ru Shih, Yi-Chun Lin, Chien-Yu

Cheng, Shu-Hsing Cheng, Yhu-Chering Huang, Tzou-Yien Lin, Jia-Tsong Jan, Che Ma, William James, Rodney S. Daniels, John W. McCauley, Pramila Rijal, Alain R. Townsend.

References

1. Polack FP, Thomas SJ, Kitchin N, Absalon J, Gurtman A, Lockhart S, et al. Safety and Efficacy of the BNT162b2 mRNA Covid-19 Vaccine. *N Engl J Med*. 2020; 383:2603–2615. <https://doi.org/10.1056/NEJMoa2034577> PMID: 33301246
2. Baden LR, El Sahly HM, Essink B, Kotloff K, Frey S, Novak R, et al. Efficacy and Safety of the mRNA-1273 SARS-CoV-2 Vaccine. *N Engl J Med*. 2021; 384:403–416. <https://doi.org/10.1056/NEJMoa2035389> PMID: 33378609
3. Bloch EM, Shoham S, Casadevall A, Sachais BS, Shaz B, Winters JL, et al. Deployment of convalescent plasma for the prevention and treatment of COVID-19. *J Clin Invest*. 2020; 130: 2757–2765. <https://doi.org/10.1172/JCI138745> PMID: 32254064
4. Li L, Zhang W, Hu Y, Tong X, Zheng S, Yang J, et al. Effect of Convalescent Plasma Therapy on Time to Clinical Improvement in Patients With Severe and Life-threatening COVID-19: A Randomized Clinical Trial. *JAMA*. 2020; 324:460–470. <https://doi.org/10.1001/jama.2020.10044> PMID: 32492084
5. Libster R, Pérez Marc G, Wappner D, Coviello S, Bianchi A, Braem V, et al. Early High-Titer Plasma Therapy to Prevent Severe Covid-19 in Older Adults. *N Engl J Med*. 2021; 384:610–618. <https://doi.org/10.1056/NEJMoa2033700> PMID: 33406353
6. Cheng Y, Wong R, Soo YO, Wong WS, Lee CK, Ng MH, et al. Use of convalescent plasma therapy in SARS patients in Hong Kong. *Eur J Clin Microbiol Infect Dis*. 2005; 24:44–46. <https://doi.org/10.1007/s10096-004-1271-9> PMID: 15616839
7. Walls AC, Park YJ, Tortorici MA, Wall A, McGuire AT, Veesler D. Structure, Function, and Antigenicity of the SARS-CoV-2 Spike Glycoprotein. *Cell*. 2020; 181:281–292.e6. <https://doi.org/10.1016/j.cell.2020.02.058> PMID: 32155444
8. Thevarajan I, Nguyen THO, Koutsakos M, Druce J, Caly L, van de Sandt CE, et al. Breadth of concomitant immune responses prior to patient recovery: a case report of non-severe COVID-19. *Nat Med*. 2020; 26:453–455. <https://doi.org/10.1038/s41591-020-0819-2> PMID: 32284614
9. Nie Y, Wang G, Shi X, Zhang H, Qiu Y, He Z, et al. Neutralizing antibodies in patients with severe acute respiratory syndrome-associated coronavirus infection. *J Infect Dis*. 2004; 190:1119–1126. <https://doi.org/10.1086/423286> PMID: 15319862
10. Long QX, Liu BZ, Deng HJ, Wu GC, Deng K, Chen YK, et al. Antibody responses to SARS-CoV-2 in patients with COVID-19. *Nat Med*. 2020; 26:845–848. <https://doi.org/10.1038/s41591-020-0897-1> PMID: 32350462
11. Lou B, Li TD, Zheng SF, Su YY, Li ZY, Liu W, et al. Serology characteristics of SARS-CoV-2 infection since exposure and post symptom onset. *Eur Respir J*. 2020; 56:2000763. <https://doi.org/10.1183/13993003.00763-2020> PMID: 32430429
12. Patrick DM, Petric M, Skowronski DM, Guasparini R, Booth TF, Krajden M, et al. An Outbreak of Human Coronavirus OC43 Infection and Serological Cross-reactivity with SARS Coronavirus. *Can J Infect Dis Med Microbiol*. 2006; 17:330–336. <https://doi.org/10.1155/2006/152612> PMID: 18382647
13. Shrock E, Fujimura E, Kula T, Timms RT, Lee IH, Leng Y, et al. Viral epitope profiling of COVID-19 patients reveals cross-reactivity and correlates of severity. *Science*. 2020; 370:eabd4250. <https://doi.org/10.1126/science.abd4250> PMID: 32994364
14. Hicks J, Klumpp-Thomas C, Kalish H, Shunmugavel A, Mehalko J, Denson JP, et al. Serologic cross-reactivity of SARS-CoV-2 with endemic and seasonal Betacoronaviruses. Preprint. medRxiv 2020.06.22.20137695. <https://doi.org/10.1101/2020.06.22.20137695> PMID: 32596697
15. Ekiert DC, Kashyap AK, Steel J, Rubrum A, Bhabha G, Khayat R, et al. Cross-neutralization of influenza A viruses mediated by a single antibody loop. *Nature*. 2012; 489:526–532. <https://doi.org/10.1038/nature11414> PMID: 22982990
16. West AP Jr, Scharf L, Scheid JF, Klein F, Bjorkman PJ, Nussenzweig MC, et al. Structural insights on the role of antibodies in HIV-1 vaccine and therapy. *Cell*. 2014; 156:633–648. <https://doi.org/10.1016/j.cell.2014.01.052> PMID: 24529371
17. Huo J, Le Bas A, Ruza RR, Duyvesteyn HME, Mikolajek H, Malinauskas T, et al. Neutralizing nanobodies bind SARS-CoV-2 spike RBD and block interaction with ACE2. *Nat Struct Mol Biol*. 2020; 27:846–854. <https://doi.org/10.1038/s41594-020-0469-6> PMID: 32661423
18. Zhou D, Duyvesteyn HME, Chen CP, Huang CG, Chen TH, Shih SR, et al. Structural basis for the neutralization of SARS-CoV-2 by an antibody from a convalescent patient. *Nat Struct Mol Biol*. 2020; 27:950–958. <https://doi.org/10.1038/s41594-020-0480-y> PMID: 32737466

19. Bruun TUJ, Andersson AC, Draper SJ, Howarth M. Engineering a Rugged Nanoscaffold To Enhance Plug-and-Display Vaccination. *ACS Nano*. 2018; 12:8855–8866. <https://doi.org/10.1021/acsnano.8b02805> PMID: 30028591
20. Barnes CO, Jette CA, Abernathy ME, Dam KA, Esswein SR, Gristick HB, et al. SARS-CoV-2 neutralizing antibody structures inform therapeutic strategies. *Nature*. 2020 Oct 12. <https://doi.org/10.1038/s41586-020-2852-1> PMID: 33045718
21. ter Meulen J, van den Brink EN, Poon LL, Marissen WE, Leung CS, Cox F, et al. Human monoclonal antibody combination against SARS coronavirus: synergy and coverage of escape mutants. *PLoS Med*. 2006; 3:e237. <https://doi.org/10.1371/journal.pmed.0030237> PMID: 16796401
22. Huo J, Zhao Y, Ren J, Zhou D, Duyvesteyn HME, Ginn HM, et al. Neutralization of SARS-CoV-2 by Destruction of the Prefusion Spike. *Cell Host Microbe*. 2020; 28:445–454.e6. <https://doi.org/10.1016/j.chom.2020.06.010> PMID: 32585135
23. Yuan M, Wu NC, Zhu X, Lee CD, So RTY, Lv H, et al. A highly conserved cryptic epitope in the receptor binding domains of SARS-CoV-2 and SARS-CoV. *Science*. 2020; 368:630–633. <https://doi.org/10.1126/science.abb7269> PMID: 32245784
24. Wrapp D, De Vlieger D, Corbett KS, Torres GM, Wang N, Van Breedam W, et al. Structural Basis for Potent Neutralization of Betacoronaviruses by Single-Domain Camelid Antibodies. *Cell*. 2020; 181:1004–1015.e15. <https://doi.org/10.1016/j.cell.2020.04.031> PMID: 32375025
25. Rijal P, Elias SC, Machado SR, Xiao J, Schimanski L, O'Dowd V, et al. Therapeutic Monoclonal Antibodies for Ebola Virus Infection Derived from Vaccinated Humans. *Cell Rep*. 2019; 27:172–186.e7. <https://doi.org/10.1016/j.celrep.2019.03.020> PMID: 30943399
26. Pinto D, Park YJ, Beltramello M, Walls AC, Tortorici MA, Bianchi S, et al. Cross-neutralization of SARS-CoV-2 by a human monoclonal SARS-CoV antibody. *Nature*. 2020; 583:290–295. <https://doi.org/10.1038/s41586-020-2349-y> PMID: 32422645
27. Zhang Y, Xu J, Jia R, Yi C, Gu W, Liu P, et al. Protective humoral immunity in SARS-CoV-2 infected pediatric patients. *Cell Mol Immunol*. 2020; 17:768–770. <https://doi.org/10.1038/s41423-020-0438-3> PMID: 32382126
28. Radbruch A, Muehlinghaus G, Luger EO, Inamine A, Smith KG, Dörner T, et al. Competence and competition: the challenge of becoming a long-lived plasma cell. *Nat Rev Immunol*. 2006; 6:741–50. <https://doi.org/10.1038/nri1886> PMID: 16977339
29. Nguyen DC, Joyner CJ, Sanz I, Lee FE. Factors Affecting Early Antibody Secreting Cell Maturation Into Long-Lived Plasma Cells. *Front Immunol*. 2019; 10:2138. <https://doi.org/10.3389/fimmu.2019.02138> PMID: 31572364
30. Klein U, Dalla-Favera R. Germinal centres: role in B-cell physiology and malignancy. *Nat Rev Immunol*. 2008; 8:22–33. <https://doi.org/10.1038/nri2217> PMID: 18097447
31. Fink K. Origin and Function of Circulating Plasmablasts during Acute Viral Infections. *Front Immunol*. 2012; 3:78. <https://doi.org/10.3389/fimmu.2012.00078> PMID: 22566959
32. Huang KA, Rijal P, Jiang H, Wang B, Schimanski L, Dong T, et al. Structure-function analysis of neutralizing antibodies to H7N9 influenza from naturally infected humans. *Nat Microbiol*. 2019; 4:306–315. <https://doi.org/10.1038/s41564-018-0303-7> PMID: 30478290
33. McIntosh K, Dees JH, Becker WB, Kapikian AZ, Chanock RM. Recovery in tracheal organ cultures of novel viruses from patients with respiratory disease. *Proc Natl Acad Sci U S A*. 1967; 57:933–940. <https://doi.org/10.1073/pnas.57.4.933> PMID: 5231356
34. Nickbakhsh S, Ho A, Marques DFP, McMenamin J, Gunson RN, Murcia PR. Epidemiology of Seasonal Coronaviruses: Establishing the Context for the Emergence of Coronavirus Disease 2019. *J Infect Dis*. 2020; 222:17–25.
35. Morfopoulou S, Brown JR, Davies EG, Anderson G, Virasami A, Qasim W, et al. Human Coronavirus OC43 Associated with Fatal Encephalitis. *N Engl J Med*. 2016; 375:497–498. <https://doi.org/10.1056/NEJMc1509458> PMID: 27518687
36. Severance EG, Bossis I, Dickerson FB, Stallings CR, Origoni AE, Sullens A, et al. Development of a nucleocapsid-based human coronavirus immunoassay and estimates of individuals exposed to coronavirus in a U.S. metropolitan population. *Clin Vaccine Immunol*. 2008; 15:1805–1810. <https://doi.org/10.1128/CVI.00124-08> PMID: 18945884
37. Dijkman R, Jebbink MF, Gaunt E, Rossen JW, Templeton KE, Kuijpers TW, et al. The dominance of human coronavirus OC43 and NL63 infections in infants. *J Clin Virol*. 2012; 53:135–139. <https://doi.org/10.1016/j.jcv.2011.11.011> PMID: 22188723
38. Beltramello M, Williams KL, Simmons CP, Macagno A, Simonelli L, Quyen NT, et al. The human immune response to Dengue virus is dominated by highly cross-reactive antibodies endowed with

- neutralizing and enhancing activity. *Cell Host Microbe*. 2010; 8:271–283. <https://doi.org/10.1016/j.chom.2010.08.007> PMID: 20833378
39. Rogers TF, Goodwin EC, Briney B, Sok D, Beutler N, Strubel A, et al. Zika virus activates de novo and cross-reactive memory B cell responses in dengue-experienced donors. *Sci Immunol*. 2017; 2:eaa6809. <https://doi.org/10.1126/sciimmunol.aaa6809> PMID: 28821561
 40. Wrammert J, Koutsonanos D, Li GM, Edupuganti S, Sui J, Morrissey M, et al. Broadly cross-reactive antibodies dominate the human B cell response against 2009 pandemic H1N1 influenza virus infection. *J Exp Med*. 2011; 208:181–193. <https://doi.org/10.1084/jem.20101352> PMID: 21220454
 41. He Y, Lu H, Siddiqui P, Zhou Y, Jiang S. Receptor-binding domain of severe acute respiratory syndrome coronavirus spike protein contains multiple conformation-dependent epitopes that induce highly potent neutralizing antibodies. *J Immunol*. 2005; 174:4908–4915. <https://doi.org/10.4049/jimmunol.174.8.4908> PMID: 15814718
 42. Robbiani DF, Gaebler C, Muecksch F, Lorenzi JCC, Wang Z, Cho A, et al. Convergent antibody responses to SARS-CoV-2 in convalescent individuals. *Nature*. 2020; 584:437–442. <https://doi.org/10.1038/s41586-020-2456-9> PMID: 32555388
 43. Cao Y, Su B, Guo X, Sun W, Deng Y, Bao L, et al. Potent Neutralizing Antibodies against SARS-CoV-2 Identified by High-Throughput Single-Cell Sequencing of Convalescent Patients' B Cells. *Cell*. 2020; 182:73–84.e16. <https://doi.org/10.1016/j.cell.2020.05.025> PMID: 32425270
 44. Liu L, Wang P, Nair MS, Yu J, Rapp M, Wang Q, et al. Potent neutralizing antibodies against multiple epitopes on SARS-CoV-2 spike. *Nature*. 2020; 584:450–456. <https://doi.org/10.1038/s41586-020-2571-7> PMID: 32698192
 45. Wu Y, Wang F, Shen C, Peng W, Li D, Zhao C, et al. A noncompeting pair of human neutralizing antibodies block COVID-19 virus binding to its receptor ACE2. *Science*. 2020; 368:1274–1278. <https://doi.org/10.1126/science.abc2241> PMID: 32404477
 46. Brouwer PJM, Caniels TG, van der Straten K, Snitselaar JL, Aldon Y, Bangaru S, et al. Potent neutralizing antibodies from COVID-19 patients define multiple targets of vulnerability. *Science*. 2020; 369:643–650. <https://doi.org/10.1126/science.abc5902> PMID: 32540902
 47. Hansen J, Baum A, Pascal KE, Russo V, Giordano S, Wloga E, et al. Studies in humanized mice and convalescent humans yield a SARS-CoV-2 antibody cocktail. *Science*. 2020; 369:1010–1014. <https://doi.org/10.1126/science.abd0827> PMID: 32540901
 48. Rogers TF, Zhao F, Huang D, Beutler N, Burns A, He WT, et al. Isolation of potent SARS-CoV-2 neutralizing antibodies and protection from disease in a small animal model. *Science*. 2020; 369:956–963. <https://doi.org/10.1126/science.abc7520> PMID: 32540903
 49. Ju B, Zhang Q, Ge J, Wang R, Sun J, Ge X, et al. Human neutralizing antibodies elicited by SARS-CoV-2 infection. *Nature*. 2020; 584:115–119. <https://doi.org/10.1038/s41586-020-2380-z> PMID: 32454513
 50. Wang C, Li W, Drabek D, Okba NMA, van Haperen R, Osterhaus ADME, et al. A human monoclonal antibody blocking SARS-CoV-2 infection. *Nat Commun*. 2020; 11:2251.
 51. Chen X, Li R, Pan Z, Qian C, Yang Y, You R, et al. Human monoclonal antibodies block the binding of SARS-CoV-2 spike protein to angiotensin converting enzyme 2 receptor. *Cell Mol Immunol*. 2020; 17:647–649. <https://doi.org/10.1038/s41423-020-0426-7> PMID: 32313207
 52. Zhu X, Liu Q, Du L, Lu L, Jiang S. Receptor-binding domain as a target for developing SARS vaccines. *J Thorac Dis*. 2013; 5 Suppl 2:S142–148. <https://doi.org/10.3978/j.issn.2072-1439.2013.06.06> PMID: 23977435
 53. Quinlan BD, Mou H, Zhang L, Guo Y, He W, Ojha A, et al. The SARS-CoV-2 receptor-binding domain elicits a potent neutralizing response without antibody-dependent enhancement. *bioRxiv* 2020.04.10.036418. <https://doi.org/10.1101/2020.04.10.036418>
 54. Yang J, Wang W, Chen Z, Lu S, Yang F, Bi Z, et al. A vaccine targeting the RBD of the S protein of SARS-CoV-2 induces protective immunity. *Nature*. 2020; 586:572–577. <https://doi.org/10.1038/s41586-020-2599-8> PMID: 32726802
 55. Shang J, Ye G, Shi K, Wan Y, Luo C, Aihara H, et al. Structural basis of receptor recognition by SARS-CoV-2. *Nature*. 2020; 581:221–224. <https://doi.org/10.1038/s41586-020-2179-y> PMID: 32225175
 56. Lan J, Ge J, Yu J, Shan S, Zhou H, Fan S, et al. Structure of the SARS-CoV-2 spike receptor-binding domain bound to the ACE2 receptor. *Nature*. 2020; 581:215–220. <https://doi.org/10.1038/s41586-020-2180-5> PMID: 32225176
 57. Wang Q, Zhang Y, Wu L, Niu S, Song C, Zhang Z, et al. Structural and Functional Basis of SARS-CoV-2 Entry by Using Human ACE2. *Cell*. 2020; 181:894–904.e9. <https://doi.org/10.1016/j.cell.2020.03.045> PMID: 32275855

58. Greaney AJ, Starr TN, Gilchuk P, Zost SJ, Binshtein E, Loes AN, et al. Complete mapping of mutations to the SARS-CoV-2 spike receptor-binding domain that escape antibody recognition. *bioRxiv* 2020.09.10.292078. <https://doi.org/10.1101/2020.09.10.292078> PMID: 32935107
59. Baum A, Fulton BO, Wloga E, Copin R, Pascal KE, Russo V, et al. Antibody cocktail to SARS-CoV-2 spike protein prevents rapid mutational escape seen with individual antibodies. *Science*. 2020; 369:1014–1018. <https://doi.org/10.1126/science.abd0831> PMID: 32540904
60. Chi X, Yan R, Zhang J, Zhang G, Zhang Y, Hao M, et al. A neutralizing human antibody binds to the N-terminal domain of the Spike protein of SARS-CoV-2. *Science*. 2020; 369:650–655. <https://doi.org/10.1126/science.abc6952> PMID: 32571838
61. Zheng Z, Monteil VM, Maurer-Stroh S, Yew CW, Leong C, Mohd-Ismail NK, et al. Monoclonal antibodies for the S2 subunit of spike of SARS-CoV-1 cross-react with the newly-emerged SARS-CoV-2. *Euro Surveill*. 2020; 25:2000291. <https://doi.org/10.2807/1560-7917.ES.2020.25.28.2000291> PMID: 32700671
62. Lip KM, Shen S, Yang X, Keng CT, Zhang A, Oh HL, et al. Monoclonal antibodies targeting the HR2 domain and the region immediately upstream of the HR2 of the S protein neutralize in vitro infection of severe acute respiratory syndrome coronavirus. *J Virol*. 2006; 80:941–950. <https://doi.org/10.1128/JVI.80.2.941-950.2006> PMID: 16378996
63. Miyoshi-Akiyama T, Ishida I, Fukushi M, Yamaguchi K, Matsuoka Y, Ishihara T, et al. Fully human monoclonal antibody directed to proteolytic cleavage site in severe acute respiratory syndrome (SARS) coronavirus S protein neutralizes the virus in a rhesus macaque SARS model. *J Infect Dis*. 2011; 203:1574–1581. <https://doi.org/10.1093/infdis/jir084> PMID: 21592986
64. Ravichandran S, Coyle EM, Klenow L, Tang J, Grubbs G, Liu S, Wang T, Golding H, Khurana S. Antibody signature induced by SARS-CoV-2 spike protein immunogens in rabbits. *Sci Transl Med*. 2020; 12:eabc3539. <https://doi.org/10.1126/scitranslmed.abc3539> PMID: 32513867
65. Klasse PJ, Moore JP. Antibodies to SARS-CoV-2 and their potential for therapeutic passive immunization. *Elife*. 2020; 9:e57877. <https://doi.org/10.7554/eLife.57877> PMID: 32573433
66. Ng KW, Faulkner N, Cornish GH, Rosa A, Harvey R, Hussain S, et al. Preexisting and de novo humoral immunity to SARS-CoV-2 in humans. *Science*. 2020; 370:1339–1343. <https://doi.org/10.1126/science.abe1107> PMID: 33159009
67. Nguyen-Contant P, Embong AK, Kanagaiah P, Chaves FA, Yang H, Branche AR, et al. S Protein-Reactive IgG and Memory B Cell Production after Human SARS-CoV-2 Infection Includes Broad Reactivity to the S2 Subunit. *mBio*. 2020; 11:e01991–20. <https://doi.org/10.1128/mBio.01991-20> PMID: 32978311
68. Lin Y, Gu Y, Wharton SA, Whittaker L, Gregory V, Li X, et al. Optimisation of a micro-neutralisation assay and its application in antigenic characterisation of influenza viruses. *Influenza Other Respir Viruses*. 2015; 9:331–340. <https://doi.org/10.1111/irv.12333> PMID: 26073976
69. Caly L, Druce J, Roberts J, Bond K, Tran T, Kostecki R, et al. Isolation and rapid sharing of the 2019 novel coronavirus (SARS-CoV-2) from the first patient diagnosed with COVID-19 in Australia. *Med J Aust*. 2020; 212:459–462. <https://doi.org/10.5694/mja2.50569> PMID: 32237278